

Concurrent object regression*

Satarupa Bhattacharjee and Hans-Georg Müller

*Department of Statistics, University of California, Davis
Davis, CA 95616 USA*

e-mail: sbhattacharjee@ucdavis.edu; hgmuller@ucdavis.edu

Abstract: Modern-day problems in statistics often face the challenge of exploring and analyzing complex non-Euclidean object data that do not conform to vector space structures or operations. Examples of such data objects include covariance matrices, graph Laplacians of networks, and univariate probability distribution functions. In the current contribution a new concurrent regression model is proposed to characterize the time-varying relation between an object in a general metric space (as a response) and a vector in \mathbb{R}^p (as a predictor), where concepts from Fréchet regression is employed. Concurrent regression has been a well-developed area of research for Euclidean predictors and responses, with many important applications for longitudinal studies and functional data. However, there is no such model available so far for general object data as responses. We develop generalized versions of both global least squares regression and locally weighted least squares smoothing in the context of concurrent regression for responses which are situated in general metric spaces and propose estimators that can accommodate sparse and/or irregular designs. Consistency results are demonstrated for sample estimates of appropriate population targets along with the corresponding rates of convergence. The proposed models are illustrated with human mortality data and resting state functional Magnetic Resonance Imaging data (fMRI) as responses.

MSC2020 subject classifications: Primary 62R20, 62J02; secondary 62G08, 62G05.

Keywords and phrases: Concurrent regression, Fréchet regression, general metric space, metric-space valued data, random objects, varying coefficient model, local regression, fMRI.

Received December 2021.

Contents

1	Introduction	4032
2	Data and model	4035
3	Nonparametric concurrent object regression	4036
4	Partially global concurrent object regression	4042
5	Simulation studies	4044
5.1	Distributional object responses	4044
5.2	Object responses on a unit sphere	4048
6	Data illustrations	4050

*Data used in preparation of this article were obtained from the Alzheimer’s Disease Neuroimaging Initiative (ADNI) database (adni.loni.usc.edu). The research of H.-G. Müller was supported by NSF grant DMS-1712864 and NSF grant DMS-2014626.

6.1	Brain connectivity in Alzheimer’s disease	4050
6.2	Impact of GDP on human mortality	4058
7	Concluding remarks	4061
A	Model diagnostic plots for ADNI data application in Section 6.1 . .	4062
B	ADNI data application in Section 6.1 using square root power metric	4062
C	Mortality-vs-GDP data application in Section 6.2 after removing out- lier observation	4063
D	Technical proofs and additional lemmas	4065
D.1	Proofs for Section 3	4065
D.2	Background for the partially global concurrent object regression	4073
D.3	Technical assumptions (B1)-(B6) and (U1)-(U4) in section 4 . .	4074
D.4	Proofs for section 4	4075
E	Additional figures	4080
	Acknowledgments	4083
	References	4084

1. Introduction

Concurrent regression models are an important tool to explore the time-dynamic nature of the dependence between two variables. They are often used in regression problems, where the effect of the covariates on the response variable is affected by a third variable, such as time or age. Specifically, the response at a particular time point is modeled as a function of the value of the covariate only at that specific time point. Concurrent regression models, also known as varying coefficient models, are natural extensions of (generalized) linear models [27, 12]. Owing to their interpretability and wide applicability in areas such as economics, finance, politics, epidemiology and the life sciences, there exists a rich literature on these models that covers a large range from simple linear models with scalar responses to more complex longitudinal and functional data [52, 24, 47, 51, 29, 60], including regression problems where both responses and covariate(s) are of functional type.

However, as we enter the era of big data, more complex, often non-Euclidean, data are increasingly observed and this motivates the development of statistical models that are suitable for such complex data. In this paper, we introduce Concurrent Object Regression (CORE) models for very general settings where one is interested in the time-varying regression relation between a response that takes values in a general metric object space without any linear structure and real-valued covariate(s). We note that no such models exist at this time and this is the first concurrent model for object data.

For the special case where the observations consist of a paired sample of square integrable random functions $(X(t), Y(t))$ that take values in \mathbb{R} , the linear functional concurrent model is well known [48] and can be written as

$$E(Y(t)|X(t)) = \mu_Y(t) + \beta(t)(X(t) - \mu_X(t)), \quad (1.1)$$

where $\mu_Y(\cdot)$ and $\mu_X(\cdot)$ are respectively the mean functions of $X(\cdot)$ and $Y(\cdot)$ and $\beta(\cdot)$ is the smooth coefficient function. This can be thought of as a series of linear regressions for each time point that are connected and restricted by the assumed smoothness of the coefficient function β .

Several methods have been proposed to estimate the model components μ_X, μ_Y and β , which are functional in nature, including local polynomial kernel smoothing regression [22, 23, 28, 64], smoothing splines [20, 11] and function approximation of $\beta(\cdot)$ through basis expansion [30]. These methods were also adapted for spatial imaging [68], ridge regression [35] and other areas. Since the linear approach may not capture the true and possibly complex nature of the relationship between Y and X , the response and the covariate, a more general nonparametric model may be preferable,

$$E(Y(t)|X(t)) = m(t, X(t)), \quad (1.2)$$

where the regression function m is assumed to satisfy some basic smoothness properties.

Unlike a linear regression model, the parametric varying coefficient model in (1.1) or the nonparametric concurrent model in (1.2) involve the nested structure of the predictor space $(T, X(T))$ and allow the regression function (the coefficient functions in the parametric model) to vary systematically and smoothly in more than one direction. We aim to capture the nested predictor space structure and develop a concurrent regression model when the responses are random objects lying in a general metric space. To the best of our knowledge, such a model has not been studied before, even though for its Euclidean analogue various methods have been discussed over the years.

Estimation and inference in the nonparametric functional concurrent regression literature include methodologies such as spline smoothing [34], Gaussian process regression [54, 62], and local kernel smoothing techniques [59] among others, with various subsequent developments [61, 74]. Regression methods have also been considered more recently for manifold-valued responses in curved spaces [73, 13, 67, 15], owing to the growing realization that data from many disciplines have manifold structures, including data generated in brain imaging, medical and molecular imaging, computational biology and computer vision.

The major objective of this paper is to overcome the limitation of Euclidean responses in the previous concurrent regression approaches, where it is always assumed that $Y(t) \in \mathbb{R}$ or $Y(t) \in \mathbb{R}^p$. The challenge that one faces in extending concurrent regression beyond Euclidean responses is that existing methodology relies in a fundamental way on the vector space structure of the responses, which is no longer available, not even locally, when responses are situated in general separable metric spaces that cover large classes of possible response types. Technological advances have made it possible to record and efficiently store time courses of image, network, sensor or other complex data. Such “object-oriented data” [36] or “random objects” [38] can be viewed as random variables taking values in a separable metric space that is devoid of a vector space structure and where only pairwise distances between the observed data are available. Such

random object data, including distributional data in Wasserstein space [39, 10], covariance matrix objects [43], data on the surface of the sphere [16], and phylogenetic trees [7], have drawn the attention of the statisticians in recent times.

As a motivating example for the proposed concurrent object regression (CORE), we consider fMRI brain-image scans for Alzheimer's patients over varying ages. It is important to note that, the space \mathcal{C} of the functional connectivity network of fMRI signals, represented as correlation matrices between the different nodes of the brain is not linear and there is no concept of direction.

However, the connectivity correlation matrices can be perceived as random objects in a metric space, endowed with a suitable metric. For example, one might be interested to see if certain measures indexing the advancement of the disease, such as the total cognitive score, are associated with the connectivity matrices. It is known that a higher total cognitive score may be linked with a more serious cognitive deficit and a higher age. At the same time, the functional connectivity itself is expected to deteriorate with increasing age as the severity of the condition intensifies over time. Of interest is then to ascertain the dependence of the functional connectivity correlation matrices of the Alzheimer's subjects on time (age) and some index of the overall health for the subjects, that also varies over time.

The space of positive semi-definite matrices is a Riemannian manifold which can be flattened locally and analyzed using linear results, however the Riemannian structure of the space depends heavily on the metric. Our approach of treating it as a metric space is more general, in the sense that it works for many metrics in the space such as the Frobenius metric, the log-Euclidean metric [3], the Procrustes metric [45, 72], the power metric [18, 19], the affine-invariant Riemannian metric [42, 37], the Cholesky metric [33] among others. As such we do not have to evoke the Riemannian geometry of the space. However, a possible challenge inherent in Fréchet regression to ascertain the existence and uniqueness of the Fréchet means may be encountered. Other examples of such general metric space objects include time-varying age-at-death densities resulting from demographic data, where the interest is in quantifying the dynamic regression relationship between the densities and time-dependent some economic index such as GDP per capita, or time-varying network data, for example internet traffic networks where one has concurrent covariates.

The natural notion of a mean for random elements of a metric space is the Fréchet mean [26]. It is a direct generalization of the standard mean, and is defined as the element of the metric space for which the expected squared distance to all other elements is minimized. It can encompass different types of means commonly used, such as the expectation, the median, or the geometric mean, and extends to non-Euclidean spaces, thus allowing for profound applications of probability theory and statistics exploiting the geometry in such spaces [50, 57, 65, 69]. [44] extended the concept of Fréchet mean to the notion of a conditional Fréchet mean, implemented as Fréchet regression, where one has samples of data (X_i, Y_i) , with the Y_i being random objects and the X_i are Euclidean predictors. This is an extension of ordinary regression to metric space valued responses.

Even though Fréchet regression [44] can incorporate a random time variable as one of the Euclidean covariates, the concurrent regression relationship between paired stochastic processes of real covariates and an object response as a function of time has not been explored yet. This is an important problem of its own accord and highly relevant in various data applications such as brain imaging for which we provide an example in Section 6.1. It is of interest to observe that concurrent object regression is not the same as Fréchet regression, just as varying coefficient models in (1.1) and (1.2) are different from linear regression models when the response is Euclidean.

In Section 3, we introduce the concurrent object regression (CORE) model for time-varying object responses and time-varying real covariate(s). We separately discuss two situations – one where we assume a “linear” dependence of the predictor and response at any given time point and a second scenario in which we assume a nonparametric model in Sections 3 and 4 respectively. Our motivating application examples deal with samples of probability distributions, data lying on unit sphere in \mathbb{R}^3 , and correlation matrices, which are illustrated with simulations and real data from neuroimaging and demography, with details in Sections 5 and 6, respectively. We conclude with a brief discussion about our methods in Section 7.

2. Data and model

Throughout, we consider a totally bounded, hence separable, metric space (Ω, d) , where the response is situated. This is coupled with a p -dimensional real valued stochastic process $X(\cdot)$ as a predictor. The Ω -valued random object response Y depends on both X and a “time”-variable $t \in \mathcal{T}$, where \mathcal{T} is a closed and bounded interval on the real line. In other words, $(X(t), Y(t)) : t \in \mathcal{T}$ are two stochastic processes that, for each given t , take values \mathbb{R}^p and Ω respectively.

A random time T is selected from some distribution f_T on \mathcal{T} , at which X is observed. Note that $X(T)$ is itself a random variable and has a probability distribution on \mathbb{R}^p . The joint distribution of $(X(T), T)$ is well defined in case $X(T)$ and T are independently distributed. For the sake of generality, we consider the joint distribution of $(X(T), T)$ and, with a slight abuse of notation, denote the joint distribution by $F_{(X,T)}$, which is a probability distribution on $\mathbb{R}^p \times \mathbb{R}$. We further assume that $Y \sim F_Y$ where F_Y is a distribution on (Ω, d) . The conditional distributions of $Y(T)|(X(T), T)$ and $(X(T), T)|Y(T)$ are denoted by $F_{Y|(X,T)}$ and $F_{(X,T)|Y}$ respectively, assuming they exist. We define the concurrent object regression (CORE) model as follows

$$m_{\oplus}(x, t) := E_{\oplus}(Y(t)|X(T) = x, T = t) := \underset{\omega \in \Omega}{\operatorname{argmin}} M_{\oplus}(\omega, x, t),$$

$$M_{\oplus}(\omega, x, t) = E(d^2(Y(t), \omega)|X(T) = x, T = t), \quad (2.1)$$

and refer to the objective function $M_{\oplus}(\cdot, x, t)$ in (2.1) as the conditional Fréchet function.

In many scenarios one does not fully observe the trajectories of responses $Y(t)$ and covariates $X(t)$. We consider a general situation, where each subject is

measured at random time points, possibly according to a sparse design, with observed data of the form $(T_{il}, X_i(T_{il}), Y_i(T_{il}))$; $l = 1, \dots, n_i$; $i = 1, \dots, n$, i.e., for the i^{th} subject one has observations of the response $Y(\cdot)$ and predictor $X(\cdot)$ at time points T_{il} that may vary from subject to subject. We denote the observed data by (T_{il}, X_{il}, Y_{il}) ; $l = 1, \dots, n_i$; $i = 1, \dots, n$. The number of observations n_i made for the i^{th} subject is a r.v. with $n_i \stackrel{i.i.d.}{\sim} N$, where $N > 0$ is a positive discrete random variable, with $E(N) < \infty$ and $P(N > 1) > 0$. The observation times and measurements are assumed to be independent of the number of measurements, i.e., for any subset $J_i \subseteq \{1, \dots, n_i\}$ and for all $i = 1, \dots, n$, $(\{T_{il} : l \in J_i\}, \{X_{il} : l \in J_i\}, \{Y_{il} : l \in J_i\})$ is independent of n_i .

3. Nonparametric concurrent object regression

In this section, we develop a nonparametric estimation strategy for the target CORE model (2.1), assuming that the dependence of the response $Y(T)$ on the predictors $X(T)$ and T , for any randomly chosen $T \in \mathcal{T}$ are local, in both directions. For ease of presentation, we provide details for the case of a scalar predictor. For the remainder of this section we will assume that $X(t) \in \mathbb{R}^p$, where $p = 1$ for all $t \in \mathcal{T}$, that is the dimension of the predictor space $(T, X(T))$, for any random time point T is $p + 1 = 2$. This allows for simpler notation and implementation. At the cost of much more involved notation, the theory can be extended to cover cases where $p > 1$.

We aim to express the CORE function $m_{\oplus}(x, t)$ in (2.1) as a weighted Fréchet mean, where the weight function varies with the values (x, t) of the predictors. The intuition behind these approaches derives from the special case of Euclidean responses.

As an illustrating motivation, let us first consider here the special case of time-varying Euclidean responses. The space is equipped with the metric $d(a, b) = d_E(a, b) = |a - b|$ for all $a, b \in \mathbb{R}$. The minimizer of M_{\oplus} in (2.1) exists, is unique and coincides with the conditional expectation, and we write

$$m_{\oplus}(x, t) = E_{\oplus}(Y(t)|X(T) = x, T = t) = E(Y(t)|X(T) = x, T = t) := m(x, t). \quad (3.1)$$

Local kernel-based nonparametric regression approaches to estimate a smooth regression function for Euclidean responses have been well investigated due to their versatility and flexibility. If we assume a nonparametric relationship of the response Y with the predictors T and $X(T)$, the local linear estimate of the function m in (3.1) at any given point (x, t) is given by $\hat{m}(x, t) := \hat{\beta}_0$. Here

$$\begin{aligned} (\hat{\beta}_0, \hat{\beta}_1, \hat{\beta}_2) = \operatorname{argmin}_{\beta_0, \beta_1, \beta_2} \frac{1}{n} \sum_{i=1}^n \left(\frac{1}{n_i} \sum_{j=1}^{n_i} (Y_{ij} - \beta_0 - \beta_1(X_{ij} - x) - \beta_2(T_{ij} - t))^2 \right) \\ \times K_{h_1, h_2}(X_{ij} - x, T_{ij} - t). \end{aligned} \quad (3.2)$$

K is a bivariate kernel function, which corresponds to a bivariate density function, and h_1, h_2 are the bandwidth parameters such that $K_{h_1, h_2}(x_1, x_2) =$

$(h_1 h_2)^{-1} K(x_1/h_1, x_2/h_2)$. We can view the above estimator in (3.2) as an M-estimator of the alternative population target

$$\begin{aligned}
 (\beta_0^*, \beta_1^*, \beta_2^*) &= \operatorname{argmin}_{\beta_0, \beta_1, \beta_2} \int \left[K_{h_1, h_2}(z - x, s - t) \right. \\
 &\quad \left. \times \left(\int y dF_{Y|X, T}(y, z, s) - \beta_0 - \beta_1(z - x) - \beta_2(s - t) \right)^2 \right] dF_{(X, T)}(z, s).
 \end{aligned}
 \tag{3.3}$$

Defining

$$\begin{aligned}
 \mu_{jk} &:= E \left(K_{h_1, h_2}(X - x, T - t)(X - x)^j (T - t)^k \right), \\
 r_{jk} &:= E \left(K_{h_1, h_2}(X - x, T - t)(X - x)^j (T - t)^k Y \right), \quad \Sigma = \begin{bmatrix} \mu_{00} & \mu_{10} & \mu_{01} \\ \mu_{10} & \mu_{20} & \mu_{11} \\ \mu_{01} & \mu_{11} & \mu_{02} \end{bmatrix},
 \end{aligned}
 \tag{3.4}$$

the solution of the minimization problem in (3.3) is

$$\tilde{l}(x, t) = \beta_0^* = [1, \quad 0, \quad 0] \Sigma^{-1} [r_{00}, \quad r_{10}, \quad r_{01}] = E \left(s^L(X, x, T, t, h_1, h_2) Y \right),
 \tag{3.5}$$

with weight function s^L given by

$$s^L(X, x, T, t, h_1, h_2) = K_{h_1, h_2}(X - x, T - t) [\nu_1 + \nu_2(X - x) + \nu_3(T - t)],
 \tag{3.6}$$

$$\begin{aligned}
 [\nu_1, \nu_2, \nu_3] &= \frac{1}{\sigma_0^2} [\mu_{20}\mu_{02} - \mu_{11}^2, \quad \mu_{01}\mu_{11} - \mu_{02}\mu_{10}, \quad \mu_{10}\mu_{11} - \mu_{20}\mu_{01}], \\
 \sigma_0^2 &= |\Sigma| = (\mu_{00}\mu_{20}\mu_{02} - \mu_{00}\mu_{11}^2 - \mu_{10}^2\mu_{02} - \mu_{01}^2\mu_{20} + 2\mu_{01}\mu_{10}\mu_{11}),
 \end{aligned}$$

where $|A|$ denotes the determinant of any square matrix A . Observing that

$\int s^L(z, x, s, t, h_1, h_2) dF_{Y, X, T}(y, z, s) = 1$, it follows that $\tilde{l}(x, t)$ in (3.5) corresponds to a localized Fréchet mean w.r.t. the Euclidean metric $d_E(a, b) := |a - b|$,

$$\tilde{l}(x, t) = \operatorname{argmin}_{y \in \mathbb{R}} E \left(s^L(X, x, T, t, h_1, h_2) d_E^2(Y, y) \right).
 \tag{3.7}$$

The minimizer $\tilde{l}(x, t)$ can be viewed as a smoothed version of the true regression function, and can therefore be treated as an intermediate target.

This locally weighted Fréchet mean in (3.7) can be readily generalized to the case of an Ω -valued stochastic process $Y(t) : t \in \mathcal{T}$, where Ω denotes a separable metric space, by retaining the same weights and replacing the Euclidean metric d_E by d . This leads to the intermediate population-level quantity, as is given below by model (3.8).

In the context of nonparametric CORE, we thus define an intermediate function $\tilde{l}_\oplus(x, t)$ as a localized weighted Fréchet mean at the chosen points (x, t) , where

$$\begin{aligned}\tilde{l}_\oplus(x, t) &:= \operatorname{argmin}_{\omega \in \Omega} \tilde{L}_\oplus(\omega, x, t), \quad \text{where} \\ \tilde{L}_\oplus(\omega, x, t) &:= E(s^L(X, x, T, t, h_1, h_2)d^2(Y, \omega)).\end{aligned}\quad (3.8)$$

Here s^L is as in (3.6) and captures the local dependence of the response on the predictor. Minimizing the intermediate objective $\tilde{L}_\oplus(\omega, \cdot, \cdot)$ in (3.8) turns out to be approximately the same as minimizing the final objective $M_\oplus(\omega)$ in (2.1). Finally, we propose an estimator for the intermediate target based on the plug-in estimates of the auxiliary parameters (see (3.4)) by their corresponding empirical estimates as follows. Define

$$\hat{\mu}_{jk} := \frac{1}{n} \sum_{i=1}^n \frac{1}{n_i} \sum_{l=1}^{n_i} K_{h_1, h_2}(X_{il} - x, T_{il} - t)(X_{il} - x)^j (T_{il} - t)^k, \quad (3.9)$$

$$\hat{\Sigma} = \begin{bmatrix} \hat{\mu}_{00} & \hat{\mu}_{10} & \hat{\mu}_{01} \\ \hat{\mu}_{10} & \hat{\mu}_{20} & \hat{\mu}_{11} \\ \hat{\mu}_{01} & \hat{\mu}_{11} & \hat{\mu}_{02} \end{bmatrix}, \quad \hat{\sigma}_0^2 = |\hat{\Sigma}|, \quad N = \sum_{i=1}^n n_i, \quad (3.10)$$

$$[\hat{\nu}_1, \hat{\nu}_2, \hat{\nu}_3] = \frac{1}{\hat{\sigma}_0^2} [\hat{\mu}_{20}\hat{\mu}_{02} - \hat{\mu}_{11}^2, \quad \hat{\mu}_{01}\hat{\mu}_{11} - \hat{\mu}_{02}\hat{\mu}_{10}, \quad \hat{\mu}_{10}\hat{\mu}_{11} - \hat{\mu}_{20}\hat{\mu}_{01}], \quad (3.11)$$

$$\hat{s}_{il}^L(x, t, h_1, h_2) = K_{h_1, h_2}(X_{il} - x, T_{il} - t) [\hat{\nu}_1 + \hat{\nu}_2(X_{il} - x) + \hat{\nu}_3(T_{il} - t)]. \quad (3.12)$$

Plugging in the above empirical estimates we obtain the local Fréchet regression estimate

$$\begin{aligned}\hat{l}_\oplus(x, t) &:= \operatorname{argmin}_{\omega \in \Omega} \hat{L}_\oplus(\omega, x, t), \quad \text{where} \\ \hat{L}_\oplus(\omega, x, t) &:= \frac{1}{n} \sum_{i=1}^n \frac{1}{n_i} \sum_{l=1}^{n_i} \hat{s}_{il}^L(x, t, h_1, h_2)d^2(Y_{il}, \omega).\end{aligned}\quad (3.13)$$

Under suitable assumptions the bias introduced by changing the true target in (2.1) to the intermediate target in (3.8), given by $d(m_\oplus(\cdot, \cdot), \tilde{l}_\oplus(\cdot, \cdot))$, converges to 0 as the bandwidths $h_1, h_2 \rightarrow 0$. In addition the stochastic term $d(\hat{l}_\oplus(\cdot, \cdot), \tilde{l}_\oplus(\cdot, \cdot))$, converges to 0 in probability, which then yields the convergence of the proposed plug-in estimator in (3.13) to the true target model in (2.1). To establish this, we require the following assumptions, which are similar to assumptions in [44].

(A1) The kernel K is symmetric around zero, with $|K_{jk}^\gamma| = |\int K^\gamma(u, v)u^k v^j dudv| < \infty$ for all $j, k = 0, 1, \dots, 6$ and $\gamma = 0, 1, 2$. Also there is a common bandwidth parameter $h > 0$, $h \rightarrow 0$, $nh \rightarrow \infty$ as $n \rightarrow \infty$, such that $h_1, h_2 \sim h$.

- (A2) The marginal density $f_{(X,T)}(x, t)$ and the conditional density $f_{(X,T)|Y}(x, t, y)$ exist and are twice continuously differentiable with uniformly bounded derivatives as a bivariate function of (x, t) , the latter for all y , for any given realization of $T = t$, $X(T) = x$, and $Y(T) = y$.
- (A3) The Fréchet means $m_{\oplus}(x, t)$, $\tilde{l}_{\oplus}(x, t)$, $\hat{l}_{\oplus}(x, t)$ exist and are unique for any given points (x, t) , and for any $\epsilon > 0$,

$$\inf_{d(\omega, m_{\oplus}(x, t)) > \epsilon} M_{\oplus}(\omega, x, t) > M_{\oplus}(m_{\oplus}(x, t), x, t).$$

- (A4) For any $\epsilon > 0$,

$$\begin{aligned} \liminf_n \inf_{d(\omega, m_{\oplus}(x, t)) > \epsilon} (M_{\oplus}(\omega, x, t) - M_{\oplus}(m_{\oplus}(x, t), x, t)) &> 0, \\ \inf_{d(\omega, \tilde{l}_{\oplus}(x, t)) > \epsilon} (\tilde{L}_{\oplus}(\omega, x, t) - \tilde{L}_{\oplus}(\tilde{l}_{\oplus}(x, t), x, t)) &> 0. \end{aligned}$$

- (A5) There exist constants $\eta_1 > 0$, $C_1 > 0$, with $d(\omega, m_{\oplus}(x, t)) < \eta_1$ such that

$$M_{\oplus}(\omega, x, t) - M_{\oplus}(m_{\oplus}(x, t), x, t) \geq C_1 d(\omega, m_{\oplus}(x, t))^2.$$

- (A6) There exist $\eta_2 > 0$, $C_2 > 0$, with $d(\omega, \tilde{l}_{\oplus}(x, t)) < \eta_2$ such that

$$\liminf_n \left[\tilde{L}_{\oplus}(\omega, x, t) - \tilde{L}_{\oplus}(\tilde{l}_{\oplus}(x, t), x, t) \right] \geq C_2 d(\omega, \tilde{l}_{\oplus}(x, t))^2.$$

- (A7) Denoting the ball of radius δ centered at $m_{\oplus}(x, t)$ by $\mathcal{B}_{\delta}(m_{\oplus}(x, t)) \subset \Omega$ and its covering number using balls of size ϵ as $N(\epsilon, \mathcal{B}_{\delta}(m_{\oplus}(x, t)), d)$,

$$\int_0^1 \sqrt{1 + \log N(\delta\epsilon, \mathcal{B}_{\delta}(m_{\oplus}(x, t)), d)} d\epsilon = O(1) \text{ as } \delta \rightarrow 0.$$

Assumptions (A1)-(A2) are necessary to show that the intermediate objective function \tilde{L}_{\oplus} is a smoothed version of the true objective function M_{\oplus} . These are assumptions akin to the ones made in [44] and are common in the nonparametric regression literature. Assumption (A3) is regarding the existence and uniqueness of the Fréchet means. The existence of the Fréchet means depends on the nature of the space, as well as the metric considered. For example, in case of Euclidean responses the Fréchet means coincide with the usual means for random vectors with finite second moments. In case of Riemannian manifolds the existence, uniqueness, and the convexity of the center of mass is guaranteed [1, 41]. In a space with a negative or zero curvature, or in a Hadamard space unique Fréchet means are also shown to exist [4, 5, 40, 55, 31].

Corresponding to each space equipped with a suitable metric, the computational challenge to find the Fréchet means could be different. In many cases, the key idea to compute the weighted Fréchet means reduces to solving a constrained quasi-quadratic optimization problem and projecting back into the solution space. For a wide class of objects such as distributions, positive semi-definite

matrices, networks, and Riemannian manifolds among others, the unique solution can be found analytically (see Propositions 1 and 2 in the Supplementary Material of [44]), and is not computationally difficult to obtain.

Assumptions (A3)–(A4) are commonly invoked to establish consistency of an M-estimator such as $\hat{m}_\oplus(x, t)$, where one uses the weak convergence of the empirical process \hat{L}_\oplus to \tilde{L}_\oplus , which in turn converges smoothly to M_\oplus . Assumptions (A5)–(A6) relate to the curvature of the objective function and are needed to control the behavior of $\tilde{L}_\oplus - M_\oplus$ and $\hat{L}_\oplus - \tilde{L}_\oplus$ respectively, near the minimum. Assumption (A7) gives a bound on the covering number of the object metric space and is satisfied by the common examples of random objects such as distributions, covariance matrices, networks and so on.

In the concurrent regression framework, an important feature of the predictor space is as follows: when $X(t) \in \mathbb{R}$, for any given $t \in \mathcal{T}$, the set $\{(t, X(t)) : t \in \mathcal{T}\}$ is a one-dimensional manifold \mathcal{M} embedded in the ambient space \mathbb{R}^2 . This is an inherent property of the whole predictor space, irrespective of the dimension (possibly $p > 1$) or the structure of $X(t)$. In our case, this reduces the effective dimension of the predictor space from two to one, i.e., the observed data (T_{il}, X_{il}) take values on this 1-dimensional manifold embedded in \mathbb{R}^2 . Note that this does not contradict our assumptions regarding the existence of the joint densities, $f_{X,T}$ (Section 2).

Denoting by $\mathcal{B}_r^{(k)}(a) \subset \mathbb{R}^k$ a ball in \mathbb{R}^k with center $a \in \mathbb{R}^k$ and radius $r > 0$, for any $t \in \mathcal{T}$ and $x = X(t)$, the center of the ball $\mathcal{B}_h^{(2)}(x, t)$ is situated on the manifold \mathcal{M} . The following assumptions ensure that the predictors are dense on \mathcal{M} .

- (A1) Assume that for any $t \in \mathcal{T}$, the number of sample points outside balls $\mathcal{B}_h^2(x, t)$ is bounded and the following asymptotic irrelevance condition hold.
- $$E \left(K^\gamma \left(\frac{X-x}{h}, \frac{T-t}{h} \right) \mathbf{1} \left((X(T), T) \notin \mathcal{B}_h^2(x, t) \right) (X-x)^j (T-t)^k \right) = O(h^{1+j+k}), \text{ for } \gamma = 0, 1, 2, \text{ where } \mathbf{1}(z \notin A) \text{ denotes the indicator function for an element } z \text{ not belonging to a set } A.$$
- (A2) The density $f_T(\cdot)$ of T is bounded away from 0 the expected number of sample points falling inside a ball $\mathcal{B}_h^2(x, t)$ of radius h centered at (x, t) for any $t \in \mathcal{T}$ and $x = X(t) \in \mathbb{R}$ is proportional to h , i.e., for some constant $c_t > 0$, $P((X_{il}, T_{il}) \in \mathcal{B}_h^2(x, t)) = c_t h$.

Assumptions akin to (A8) are encountered in local polynomial regression [6, 21] to facilitate enough sample points to ensure estimation accuracy of the proposed methods. In particular it holds for a kernel K with exponential tails. Assumption (A9) concerns the existence of a local “chart” or homeomorphism from a neighborhood in the predictor space \mathbb{R}^2 to a ball in \mathbb{R} , along the curve $\{(t, X(t)) : t \in \mathcal{T}\}$. This manifold structure of the predictor space is crucial to show that the rate of convergence corresponds to that for 1-dimensional predictors even though the predictor dimension is \mathbb{R}^2 . For a generalization of the nonparametric CORE, where $X(t) \in \mathbb{R}^p$, for $p > 1$ and for any $t \in \mathcal{T}$, this observation still holds true and can be used to reduce the effective predictor

dimension by one.

The following propositions demonstrate that, while we have a *two dimensional* predictor (X, T) , the rate of convergence of the proposed estimator still corresponds to the known optimal rate for a nonparametric regression with a *one-dimensional* predictor. A similarly reduced rate of convergence is obtained for a p -dimensional Euclidean predictor X . The reason that the effective predictor dimension is p and not $(p + 1)$ is the manifold constraint. Proposition 3.1 shows that the bias introduced by changing the concurrent object regression model $m_{\oplus}(\cdot, \cdot)$ in (2.1) to the intermediate nonparametric version of the CORE model $\tilde{l}_{\oplus}(\cdot, \cdot)$ in (3.8) is negligible for a large enough sample size, if the bandwidth parameter for the bivariate kernel is chosen sufficiently small as a function of the sample size. Proposition 3.2 is about the stochastic convergence of the nonparametric CORE estimator $\hat{l}_{\oplus}(\cdot, \cdot)$ in (3.13).

Proposition 3.1. *Under the regularity assumptions (A1)-(A6), for any given points $t \in \mathcal{T}$ and $x = X(t) \in \mathbb{R}$,*

$$d(m_{\oplus}(x, t), \tilde{l}_{\oplus}(x, t)) = O(h^2), \text{ as } h = h_n \rightarrow 0, nh \rightarrow \infty,$$

where h is as in (A1) and $n \rightarrow \infty$.

Proposition 3.2. *Under the regularity assumptions (A1)-(A9), for any given points $t \in \mathcal{T}$ and $x = X(t) \in \mathbb{R}$,*

$$d(\hat{l}_{\oplus}(x, t), \tilde{l}_{\oplus}(x, t)) = O_p((nh)^{-1/2}), \text{ as } h = h_n \rightarrow 0, nh \rightarrow \infty,$$

where h is as in (A1) and $n \rightarrow \infty$.

In general, the rate of convergence is dictated by the local geometry of the object space near the minimum as quantified in (A4)-(A6). The derivations for the pointwise results are in the Appendix D.1 and like Theorem 3 and Theorem 4 of [44], rely on tools from the theory of M-estimation. Combining these two results leads to the overall rate of convergence of the nonparametric CORE estimator.

Theorem 3.1. *Under the regularity conditions (A1)-(A9),*

$$d(m_{\oplus}(x, t), \hat{l}_{\oplus}(x, t)) = O_p\left(h^2 + (nh)^{-\frac{1}{2}}\right),$$

as $h = h_n \rightarrow 0, nh \rightarrow \infty$ and $n \rightarrow \infty$.

Under the Assumptions (A1)-(A9), if we consider a sequence of bandwidths of the form $h = n^{-\gamma}$, the optimal choice for γ that minimizes the mean square error is obtained for $\gamma^* = 1/5$ and the resulting rate of convergence is

$$d(m_{\oplus}(x, t), \hat{l}_{\oplus}(x, t)) = O_p(n^{-2/5}).$$

The nonparametric CORE model and assumptions considered so far are developed for the case $X(\cdot) \in \mathbb{R}$. For instance, the kernel is assumed to be bivariate, and the weights s^L in (3.6) and their estimates in (3.12) accommodate a real-valued predictor process. The theory can be generalized for $p > 1$, however,

there are practical limitations, including the curse of dimensionality, multiple bandwidth choices, and one has to account for correlation and differences in scale between the components of $X(\cdot)$. Under more stringent modeling assumptions some of these issues can be avoided by a modeling approach that extends the notion of linear relationship to the X direction and this will be discussed next section.

4. Partially global concurrent object regression

In the Euclidean case, a well-established alternative to nonparametric concurrent regression is a global/linear varying coefficient model, where for each fixed time a linear regression of $Y(\cdot)$ on $X(\cdot)$ is assumed. This linear regression relation can be described by a global weight function applied to the covariate $X(\cdot)$. This can then be adapted for the case where responses are random objects, by constructing conditional Fréchet means with this same weight function [44], all while assuming nonlinear dependence between $Y(T)$ and T . As before, we first study the special case of a Euclidean response and then express the CORE function in (2.1) as an intermediate target expressed as a weighted Fréchet mean, the weights being globally linear in the X -direction and locally linear in the T -direction. The partially linear dependence in the X -direction imposes a more structural model than the general conditional Fréchet mean defined in (2). This leads to the proposed partially global concurrent object regression model, with the Euclidean predictor $X(\cdot) \in \mathbb{R}^p$, ($p \geq 1$) and object response $Y(\cdot) \in \Omega$, at the given points $T = t$ and $X(T) = x$ as

$$\tilde{g}_{\oplus}(x, t) = \operatorname{argmin}_{\omega \in \Omega} \tilde{G}_{\oplus}(\omega, x, t), \quad \text{where } \tilde{G}_{\oplus}(\omega, x, t) := E(s^G(X, x, T, t, h)d^2(Y, \omega)). \quad (4.1)$$

Here the weight function s^G is given by

$$s^G(z, x, s, t, h) = s_1(z, x, s, t, h) + s_2(s, t, h), \quad (4.2)$$

with $s_1(z, x, s, t, h) := K_h(s - t) [(z - \mu_X(t))^{\top} \Sigma_{20}^{-1} (x - \mu_X(t))]$, where $\mu_X(t) = E(X(t)) = E(X|T = t)$, and $s_2(s, t, h) := \frac{1}{\sigma_0^2} K_h(s - t) (\mu_{02} - (s - t)\mu_{01})$. For the explicit derivation of the weight function s^G , motivated from the special case of time-varying Euclidean responses, please refer to Appendix D.4. Here s^G encapsulates the dependence of the response on the predictors, where the dependence is global in the direction of the covariate X , while it is local in the T direction, which is reflected in the two parts $s^G(z, x, s, t, h) = s_1(z, x, s, t, h) + s_2(s, t, h)$.

The partially global CORE model imposes more structure in the predictor space of X and is less flexible than the nonparametric concurrent object regression in this sense. However, if there is a global dependence on X , for example, if the relationship between the response Y and the predictor X follows a geodesic path, the partially global model is preferable to the nonparametric version. In

addition, the partially global CORE is useful for a higher dimensional predictor in the sense that it provides a more stable estimation method and avoids the curse of dimensionality, from which the nonparametric model suffers inherently. In practice, one should implement a partially global or a nonparametric CORE method by checking whichever method results in a smaller prediction error. The computation of the root mean squared prediction error for positive semi definite matrix objects for the Frobenius norm is illustrated in (6.3) in Section 6.1.

Observe that $s_1(\cdot, \mu_X(t), \cdot, \cdot, \cdot) = 0$, that is, the regression model reduces to a nonparametric regression model with the only predictor T when $x = \mu_X(t)$. We see that $\int s_1(z, x, s, t, h) dF_{(X,T)}(z, s) = 0$. Also, under mild assumptions (Assumption B1 in the Appendix D.3) on the kernel $K_h(\cdot)$ and the smoothness of marginal and conditional densities $f_{(X,T)}$ and $f_{(X,T)|Y}$ we can show that (see the Appendix D.4) $\int s_2(s, t, h) dF_{X,T|Y}(z, s, y) = \frac{dF_{X,T|Y}(z, s, y)}{dF_{X,T}(z, s)} + O(h^2)$. Thus we may view \tilde{G}_\oplus as a smoothed version of M_\oplus as the bandwidth parameter $h = h_n \rightarrow 0$ (see the Appendix D.4).

Finally, we propose a plug-in estimate for the partially-global regression model g_\oplus in (4.1). For this purpose we define the preliminary estimates of the auxiliary parameters as follows

$$\hat{\mu}_{0j} := \frac{1}{n} \sum_{i=1}^n \frac{1}{n_i} \sum_{l=1}^{n_i} K_h(T_{il} - t)(T_{il} - t)^j, \tag{4.3}$$

$$\hat{\Sigma}_{2j} := \frac{1}{n} \sum_{i=1}^n \frac{1}{n_i} \sum_{l=1}^{n_i} K_h(T_{il} - t)(T_{il} - t)^j (X_{il} - \hat{\mu}_X(t))(X_{il} - \hat{\mu}_X(t))^T, \tag{4.4}$$

$$\hat{\sigma}_0^2 := \hat{\mu}_{02}\hat{\mu}_{00} - \hat{\mu}_{01}^2. \tag{4.5}$$

The mean function $\mu_X(\cdot)$ for the predictor process $X(\cdot)$ is estimated by $\hat{\mu}_X(\cdot)$ by smoothing the aggregated data (T_{il}, X_{il}) $i = 1, \dots, n, j = 1, \dots, n_i$, with local linear fitting [66]. We then calculate empirical weights using the auxiliary parameters from above as

$$\begin{aligned} \hat{s}_{il}^G(x, t, h) &= K_h(T_{il} - t)[(X_{il} - \hat{\mu}_X(t))^T \hat{\Sigma}_{20}^{-1} (x - \hat{\mu}_X(t)) \\ &\quad + \frac{1}{\hat{\sigma}_0^2} (\hat{\mu}_{02} - (T_{il} - t)\hat{\mu}_{01})]. \end{aligned} \tag{4.6}$$

The proposed partially global concurrent object regression (CORE) estimate is given by

$$\begin{aligned} \hat{g}_\oplus(x, t) &:= \operatorname{argmin}_{\omega \in \Omega} \hat{G}_\oplus(\omega, x, t), \text{ where} \\ \hat{G}_\oplus(\omega, x, t) &:= \frac{1}{n} \sum_{i=1}^n \left(\frac{1}{n_i} \sum_{l=1}^{n_i} \hat{s}_{il}^G(x, t, h) d^2(Y_{il}, \omega) \right). \end{aligned} \tag{4.7}$$

Further motivation of this approach, starting from the case of Euclidean responses, can be found in the Appendix D.2. We show consistency with an optimal rate for the proposed model to the target CORE function in (2.1) under

assumptions (B1)–(B6) (see the Appendix D.3), which are similar to the assumptions (A1)–(A6) in Section 3.

Proposition 4.1. *Under the assumptions (B1)–(B3), for any given points $t \in \mathcal{T}$ and $x = X(t) \in \mathbb{R}^p$,*

$$d(m_{\oplus}(x, t), \tilde{g}_{\oplus}(x, t)) = O(h^2), \text{ as } h = h_n \rightarrow 0 \text{ and } n \rightarrow \infty.$$

Proposition 4.2. *Under the assumptions (B1)–(B6), for any given points $t \in \mathcal{T}$ and $x = X(t) \in \mathbb{R}^p$,*

$$d(\hat{g}_{\oplus}(x, t), \tilde{g}(x, t)) = O_p((nh)^{-1/2}), \text{ as } h = h_n \rightarrow 0, \text{ } nh \rightarrow \infty, \text{ and } n \rightarrow \infty.$$

Combining these two results leads to the pointwise consistency for the partially global CORE estimator as follows:

Theorem 4.1. *Under Assumptions (B1)–(B6),*

$$d(\hat{g}_{\oplus}(x, t), m_{\oplus}(x, t)) = O_p(h^2 + (nh)^{-1/2}),$$

as $h = h_n \rightarrow 0$, $nh \rightarrow \infty$, and $n \rightarrow \infty$.

Comparing to the local rates of convergence for the nonparametric CORE estimator, as proposed in Section 3, the rates in Propositions 4.1 and 4.2 are global in the predictor X and remain unchanged even for a higher predictor dimension p , $p > 1$. For $p = 1$, both the estimators behave in a similar manner, however as p increases the partially global estimator performs better in terms of the rate of convergence to the true CORE model in (2.1). While the above results are pointwise, a uniform convergence result in a compact interval in the X -direction also holds for any given point in the T -direction, under slightly stronger assumptions (see assumptions (U1)–(U4) in the Appendix D.3). Denoting the Euclidean norm on \mathbb{R}^p by $\|\cdot\|_E$, we obtain

Theorem 4.2. *Under the assumptions (U1)–(U4), for any given $t \in \mathcal{T}$ and $M > 0$,*

as $h = h_n \rightarrow 0$ and $nh \rightarrow \infty$,

$$\sup_{\|x\|_E \leq M} d(\hat{g}_{\oplus}(x, t), m_{\oplus}(x, t)) = O_p\left(h^2 + (nh)^{-1/2+\delta}\right), \text{ for any } \delta > 0.$$

The proofs require results from empirical process theory (see the Appendix D.4).

5. Simulation studies

5.1. Distributional object responses

We illustrate the efficacy of the proposed methods through simulations, where the space of distributions with the Wasserstein metric provides an ideal setting.

We consider time-varying distributions on a bounded domain \mathcal{T} as the response, $Y(\cdot)$, and they are represented by the respective quantile functions $Q(Y)(\cdot)$. The time-varying Euclidean random variable $X(\cdot)$ is taken as the predictor. The random response is generated conditional on $(X(T), T)$, by adding noise to the true regression quantile

$$Q(m_{\oplus}(x, t))(\cdot) = E(Q(Y)(\cdot)|X(t) = x, T = t). \tag{5.1}$$

Two different simulation scenarios are examined as we generate the distribution objects from location-scale shift families (see Table 1). In the first setting, the response is generated, on average, as a normal distribution with parameters that depend on $(T, X(T))$. For $T = t$, $X(T) = x$, the distribution parameters $\mu \sim N(\zeta(x, t), \nu_1)$ and $\sigma \sim \text{Gamma}\left(\frac{\eta^2(x, t)}{\nu_2}, \frac{\nu_2}{\eta^2(x, t)}\right)$ are independently sampled. The corresponding distribution is given by $Q(Y)(\cdot) = \mu + \sigma\Phi^{-1}(\cdot)$. Here, the relevant sub-parameters are chosen as $\nu_1 = 0.1$, $\nu_2 = 0.1$, $\zeta(x, t) = 0.5 + 0.1x + 0.1t^2$, and $\eta(x, t) = 0.5 + 0.1x + 0.1 \sin(10\pi t)$, and $\Phi(\cdot)$ is the standard normal distribution function.

The second setting is slightly more complicated. The distributional parameter $\mu|X(t) = x, T = t$ is sampled as before and $\sigma = 0.1$ is assumed to be a fixed parameter. The resulting distribution is then “transported” in Wasserstein space \mathcal{W} via a random transport map T , that is uniformly sampled from the collection of maps $T_k(a) = a - \sin(ka)/|k|$ for $k \in \pm 1, \pm 2$. The distributions thus generated are not Gaussian anymore due to the transportation. Nevertheless, one can show that the Fréchet mean is exactly $\mu + \sigma\Phi^{-1}(\cdot)$ as before.

TABLE 1
Table showing two different simulation scenarios.

Setting I	Setting II
$Q(Y)(\cdot) = \mu + \sigma\Phi^{-1}(\cdot)$, where $\mu \sim N(\zeta(x, t), \nu_1)$ $\sigma \sim \text{Gamma}\left(\frac{\eta^2(x, t)}{\nu_2}, \frac{\nu_2}{\eta^2(x, t)}\right)$	$Q(Y)(\cdot) = T\#(\mu + \sigma\Phi^{-1}(\cdot))$, where $\mu \sim N(\zeta(x, t), \nu_1)$ $\sigma = 0.1$, $T_k(a) = a - \sin(ka)/ a , k \in \{\pm 1, \pm 2\}$

In Table 1, $T\#p$ is a push-forward measure such that $T\#p(A) = p(\{x : T(x) \in A\})$, for any measurable function $T : \mathbb{R} \rightarrow \mathbb{R}$, distribution $p \in \mathcal{W}$, and set $A \subset \mathbb{R}$. Here the random transport map T is uniformly sampled from the collection of maps $T_k(a) = a - \sin(ka)/|a|, k \in \{\pm 1, \pm 2\}$, p is a Gaussian distribution with parameters μ and σ as described in above, and \mathcal{W} is the metric space of distributions equipped with the Wasserstein metric.

To this end, we generated a random sample of size n of time-varying response and predictors from the true models, where the i^{th} sample was observed at n_i random time points, incorporating measurement error as described in the two situations above. For simplicity, we chose $n_i = m$ to be equal for all subjects and consider the two cases with $n_i = 5$ and $n_i = 20$. Each such case was repeated for sample sizes $n = 100$ and $n = 1000$. For a given n_i and n , we first sampled the time points $T_{il} \stackrel{i.i.d.}{\sim} \text{Unif}(0, 1)$ for $l = 1, \dots, n_i$ and $i = 1, \dots, n$. The predictor

trajectories $X_i(\cdot)$ were generated as follows. The simulated processes X had the mean function $\mu_X(t) = t + \sin(t)$, with covariance function constructed from $K = 10$ eigen functions, $\phi_1(t) = -\cos(\pi t/10)/\sqrt{5}$, and $\phi_j(t) = \sin((2j-1)\pi t/10)/\sqrt{5}$, for $t \in [0, 1]$, $j = 2, \dots, K$. We chose $\lambda_1 = 1$, $\lambda_2 = .7$, to be the first two eigen values and $\lambda_j = (0.7)^{j-1}$ for $j = 3, \dots, K$ as the remaining eigenvalues. The FPC scores ξ_{ij} s were generated from $N(0, \lambda_j)$ truncated on $[-6, 6]$ for $j = 1 \dots, K$. Using the Karhunen–Loève theorem, the predictor process is generated at the random time-points $T + il$ as $X_i(T_{il}) = \mu_X(T_{il}) + \sum_{j=1}^K \xi_{ij} \phi_j(T_{il})$ for $l = 1 \dots, n_i$ and $i = 1 \dots, n$.

For each of Setting I and II, 500 Monte Carlo runs were executed for a combination of sample sizes n and n_i , including both sparse and dense designs. For the r^{th} simulation, $\hat{f}_{\oplus}^r(x, t)$ denoting the fitted distribution function, and $f_{\oplus}^r(x, t)$ denoting the simulated density objects, the utility of the estimation was measured quantitatively by the integrated squared errors

$$\text{ISE}_r = \int_0^1 \int_{-6}^6 d_W^2(\hat{f}_{\oplus}^r(x, t), f_{\oplus}^r(x, t)) dx dt, \quad (5.2)$$

where d_W denotes the Wasserstein metric between two distributions.

We fitted both of the nonparametric and partially global concurrent object regression (CORE) models over a grid of points $x = x(t) \in [-6, 6]$ and $t \in [0, 1]$. The bandwidths for the estimation in both the settings were chosen over a grid of possible values using a cross validation criterion so as to minimize the average ISE for all simulations. For the x - direction a grid of bandwidths $h_2 \in [n^{-1/5}, 3.18n^{-1/5}]$ was used for this purpose, while for the t - direction a grid of bandwidths $h_1 \in [0.05n^{-1/5}, 0.265n^{-1/5}]$ was used. A truncated bivariate Gaussian product kernel and a truncated univariate Gaussian kernel were chosen to fit the nonparametric CORE and the partially global CORE methods, respectively.

In Setting I, the performances of the proposed CORE models were compared to a baseline linear concurrent model, which is mis-specified in our case. As such, since in the first setting we knew the finite-dimensional generating model, we computed the mean $\mu_i(T_{il})$ and standard deviation $\sigma_i(T_{il})$ of the distribution Y_{il} and regressed each of them linearly against the predictors (X_{il}, T_{il}) . The quantile functions for the baseline model was computed as $\hat{\mu}(x, t) + \hat{\sigma}(x, t)\Phi^{-1}(\cdot)$, where $\hat{\mu}(x, t)$ and $\hat{\sigma}(x, t)$ were the estimated mean and variance functions at (x, t) using the fitted coefficients from the previous step. Clearly, the baseline concurrent model is mis-specified, but it highlights the fact that the proposed CORE models are the only applicable regression model, to the best of our knowledge, in the context of concurrent regression for distributional object responses. We also compared the performance of the CORE models to that of the global Fréchet regression (GFR) model [44] where T and X were used as a two-dimensional predictor, ignoring the inherent nested structure of the predictor space $(T, X(T))$. We observed a decrease in ISE for all the models as the sample size was increased, favorably for the denser design with $n_i = 20$ (see Figure 1). The CORE models outperformed both the baseline (mis-specified) model and the GFR model.

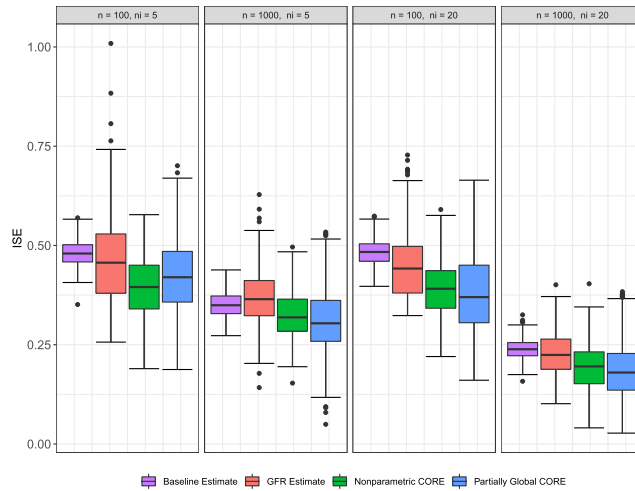


FIG 1. Boxplots of Integrated Squared Errors (ISE) over 500 simulation runs and different sample sizes for density estimates resulting from partially global and nonparametric concurrent object regression (CORE), global Fréchet regression (GFR) and a baseline model in the simulation setting I, as described in Table 1.

Further, the partially global CORE had slightly lower ISE value than the nonparametric one, specially for denser designs. In this setting either of the CORE model can be implemented to get a small ISE. In fact, the GFR model also gives reasonable estimates except for some outliers. This can be expected since in this simulation setting, the global model holds true in the x - direction.

Further, under simulation Setting-I, the performance of the proposed partially global concurrent object regression (CORE) model is compared to the global Fréchet regression (GFR) method for distributional object responses with increasing the predictor dimension p in Figure 16 of Appendix E.

In the second simulation setting, the baseline linear model is no longer admissible due to the random transportation step, thus the baseline model is dropped for the comparison purpose. However, we could still compare the performances among the two proposed CORE models and the GFR model. Both CORE methods performed in a similar manner and outperformed the GFR in all scenarios (see Figure 2). We again observed a decreasing pattern of the integrated squared errors for increasing sample sizes and denser designs, demonstrating the validity of the CORE models for this complex and time-varying regression setting. The nonparametric CORE performed better for a higher sample size. This is not unexpected since the data generating mechanism was non-linear and the partially global model assumes a linear dependence in the x - direction. The simulation Setting-II shows the relative efficiency of the nonparametric CORE versus the partially global CORE and GFR for a non-linear structure of the predictor space.

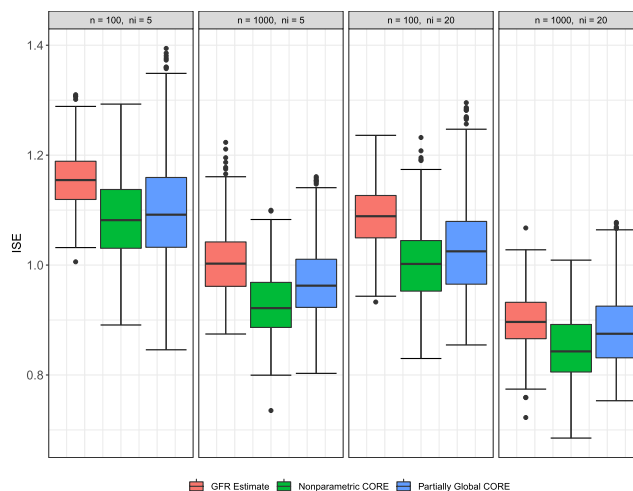


FIG 2. Boxplots of Integrated Squared Errors (ISE) for 500 simulation runs and different sample sizes for density estimates resulting from partially global and nonparametric concurrent object regression (CORE) and global Fréchet regression (GFR) for simulation setting II, as described in Table 1.

5.2. Object responses on a unit sphere

We next implemented our methodology when the responses lie on a Riemannian manifold object space – in particular we considered responses lying on the surface of a unit sphere S^2 in \mathbb{R}^3 with the center being the origin. The geodesic distance between any two points ω_1 and ω_2 lying on the surface of the unit sphere S^2 is given by $d(\omega_1, \omega_2) = \arccos(\omega_1^T \omega_2)$. We considered the concurrent object regression function as follows

$$m_{\oplus}(x, t) = ((1 - (x/a)^2)^{1/2} \cos(\pi t), (1 - (x/a)^2)^{1/2} \sin(\pi t), (x/a)), \\ t \in (0, 1), x \in (-a, a), a > 0.$$

We first generated the predictor process $(T_{il}, X_i(T_{il}))$ as before (see Section 5.1) such that $T_{il} \in (0, 1)$ and $X_i(T_{il}) \in (-a, a)$ with $a = 6$ for $l = 1, \dots, n_i$, $i = 1 \dots, n$. The response was then constructed as follows. A bivariate noise random vector was generated on the tangent space $T_{m_{\oplus}(X_{il}, T_{il})}(\Omega)$. To this end, we defined $\psi_{il} = \arcsin(T_{il})$ and $\theta_{il} = \pi T_{il}$. An orthonormal basis for the tangent space was denoted by (b_{1il}, b_{2il}) , where $b_{1il} = (\cos(\psi_{il}) \cos(\theta_{il}), \cos(\psi_{il}) \sin(\theta_{il}), -\sin(\psi_{il}))^T$ and $b_{2il} = (\sin(\theta_{il}), -\cos(\theta_{il}), 0)^T$. Adding a noise level $\sigma^2 = 0.1$, bivariate random vectors $Z_{il} = c_{i1}b_{1il} + c_{i2}b_{2il}$ were computed, where $C_i = (c_{i1}, c_{i2})^T \stackrel{i.i.d.}{\sim} N_2(0, \sigma^2 I_2)$ with $\sigma^2 = 0.1$. Finally, the response was constructed as

$$Y_{il} = \cos(\|Z_{il}\|_E) m_{\oplus}(X_{il}, T_{il}) + \sin(\|Z_{il}\|_E) \frac{Z_{il}}{\|Z_{il}\|_E},$$

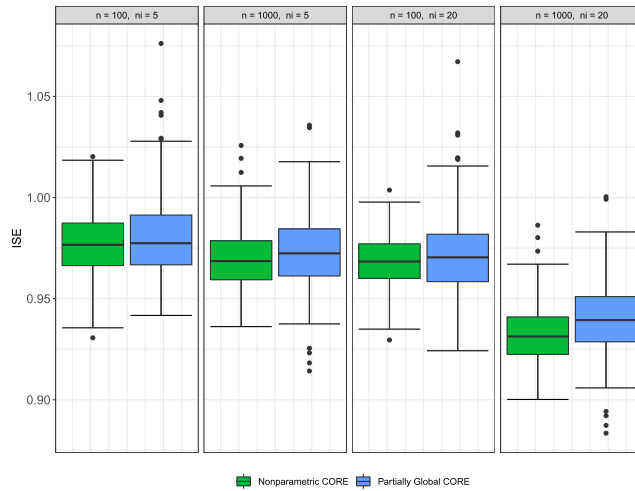


FIG 3. Boxplots of Integrated Squared Errors (ISE) for 500 simulation runs and different sample sizes for object responses on the surface of the unit sphere S^2 resulting from partially global and nonparametric concurrent object regression (CORE).

with $\|\cdot\|_E$ being the Euclidean norm. The simulation steps produced a point Y_{il} on the surface of the two-dimensional sphere with conditional Fréchet mean $m_{\oplus}(X_{il}, T_{il})$ contaminated with a small level of noise.

We fitted the two concurrent object regression (CORE) models for the simulated data over a grid of points $x(t) = x \in (-6, 6)$ and $t \in (0, 1)$. For each of the CORE models, 500 Monte Carlo runs were implemented corresponding to combinations of sample sizes n and n_i , including both sparse and dense designs. For the r^{th} simulation, at any given point (x, t) , $Y_{\oplus}^r(x, t)$ and $\hat{Y}_{\oplus}^r(x, t)$ denoted the simulated and fitted objects on the surface of the unit sphere S^2 . The performance of the model was measured quantitatively by the integrated squared errors

$$\text{ISE}_r = \int_0^1 \int_{-6}^6 d_g^2(\hat{Y}_{\oplus}^r(x, t), Y_{\oplus}^r(x, t)) dx dt, \quad (5.3)$$

where d_g denotes the geodesic distance on a unit sphere S^2 . The bandwidths for the estimation were chosen using a cross validation criterion so as to minimize the average ISE over all simulations, and a truncated Gaussian kernel was chosen. Figure 3 shows that, as before, with an increasing sample size and denser design the average ISE reduces for both nonparametric and partially global CORE models. In this simulation scenario, both the partially global and nonparametric concurrent object regression (CORE) methods work comparably and reasonably well in terms of lower estimation error. The partially global CORE method works slightly better, especially for a larger sample size and dense design. The outliers present seem to influence the mean ISEs. We report the median of the ISEs as a more robust measure, along with the mean ISEs for

varying sample sizes in Table 2.

TABLE 2

Table displaying the mean and median Integrated Squared Errors (ISE)s for object responses on the surface of the unit sphere S^2 resulting from partially global and nonparametric concurrent object regression (CORE), as described in Figure 3.

		$n = 100$ $n_i = 5$	$n = 100$ $n_i = 20$	$n = 1000$ $n_i = 5$	$n = 100$ $n_i = 20$
Nonparametric CORE	Mean	0.9764	0.9685	0.9688	0.9407
	Median	0.9766	0.9683	0.9686	0.9394
Partially global CORE	Mean	0.9811	0.9713	0.9737	0.9316
	Median	0.9774	0.9704	0.9724	0.9313

6. Data illustrations

6.1. Brain connectivity in Alzheimer's disease

Modern functional Magnetic Resonance Imaging (fMRI) methodology has made it possible to study structural elements of the brain and identify brain regions or cortical hubs that exhibit similar behavior, especially when subjects are in the resting state [2, 25]. In resting state fMRI, a time series of Blood Oxygen Level Dependent (BOLD) signal is observed for the seed voxels in selected functional hubs. For each hub, a seed voxel is identified as the voxel whose signal has the highest correlation with the signals of nearby voxels. Alzheimer's Disease has been found to have associations with anomalies in functional integration of brain regions and target regions or hubs of high connectivity in the brain [14, 70].

Data used in the preparation of this article were obtained from the Alzheimer's Disease Neuroimaging Initiative (ADNI) database (adni.loni.usc.edu). For up-to-date information, see www.adni-info.org. Brain image-scans for subjects in different stages of the disease were available, along with other relevant information such as age, gender, and total cognitive score, recorded on the same date as the scan.

For this analysis, subjects aged from 50 to 90 years and belonging to either of the Alzheimer's Disease (AD) or Cognitive Normal (CN) patient groups were considered. After removing the outliers, the number of image scans recorded were 174 and 694, respectively, for the 78 AD subjects and 371 CN subjects who participated in the study. To confirm that the age intervals across the two groups are comparable, we first performed a Kruskal- Wallis test for the null hypothesis of equal age distributions of the two groups, which resulted in a p-value of 0.92, indicating no evidence for systematic age differences.

BOLD signals for $V = 10$ brain seed voxels for each subject were extracted. The 10 hubs where the voxels are situated are labeled as follows: LMF and RMF (left and right middle-frontal), LPL and RPL (left and right parietal), LMT and RMT (left and right middle temporal), MSF (medial superior frontal), MP (medial prefrontal), PCP (posterior cingulate/precuneus) and RS (right supramarginal), as discussed in [9].

The preprocessing of the BOLD signals was implemented by adopting the standard procedures of slice-timing correction, head motion correction and normalization and other standard steps. The signals for each subject were recorded over the interval $[0, 270]$ (in seconds), with $K = 136$ measurements available at 2 second intervals. From this the temporal correlations were computed to construct the connectivity correlation matrix, also referred to as the Pearson correlation matrix in the area of fMRI studies.

The observations were available sparsely at random time-points, such that the i^{th} subject is observed at n_i time-points, n_i varying from a minimum of 1 to a maximum of 7. The inter-hub connectivity Pearson correlation matrix Y_{il} , for the i^{th} subject observed at age T_{il} (measured in years), has the $(q, r)^{\text{th}}$ element

$$(Y_{il})_{qr} = \frac{\sum_{p=1}^K (s_{ipq} - \bar{s}_{iq})(s_{ipr} - \bar{s}_{ir})}{\left[\left(\sum_{p=1}^K (s_{ipq} - \bar{s}_{iq})^2 \right) \left(\sum_{p=1}^K (s_{ipr} - \bar{s}_{ir})^2 \right) \right]^{1/2}}, \quad (6.1)$$

where s_{ipq} is the $(p, q)^{\text{th}}$ element of the signal matrix for the i^{th} subject and $\bar{s}_{iq} := \frac{1}{K} \sum_{p=1}^K s_{ipq}$ is the mean signal strength for the q^{th} voxel.

For Alzheimer's disease trials, ADAS-Cog-13 is a widely-used measure of cognitive performance. It measures impairments across several cognitive domains that are considered to be affected early and characteristically in Alzheimer's disease [49, 32]. It is important to note that higher scores are associated with more serious cognitive deficiency. To study how functional connectivity in the brain varies with the total cognitive score for subjects at different ages, we applied the CORE models. It is known that age affects both functional connectivity in the brain and total cognitive score so that the relation of cognitive deficits with brain connectivity likely changes with age.

We implemented a time-varying or concurrent regression framework with the Pearson correlation matrices in (6.1) as time-varying object responses, residing in the metric space of correlation matrices equipped with the Frobenius norm, and total cognitive scores as real-valued covariates, changing with time (age in years).

The Frobenius norm in the space of positive semi-definite matrices is related to a near linear/Euclidean metric. However, the weight function in the concurrent object regression (CORE) models can assume negative values, especially near the boundary, and the optimization algorithm in the CORE models requires us to project back into the metric space (Ω, d) . This facilitates extrapolation for points outside the dataset, though for this application we do not implement it.

The structure of the space and the results of the concurrent regression (CORE) methods depend on the choice of the metric. The metric can be chosen for the appropriate interpretability in the context of the specific data application. For the ADNI data application in this section the Frobenius metric is a suitable choice owing to the interpretable results. Another common and useful choice of metric for the space of positive semi-definite matrices is the square-root power metric [56, 17, 53, 45]. A comparative illustration is given in Appendix B in the context of the ADNI data, where the CORE models are implemented using the

TABLE 3
Bandwidths used in the nonparametric CORE model for the AD and CN subjects, here h_1 is the bandwidth for age and h_2 for total cognitive score.

	AD	CN
h_1	3.95	3.64
h_2	3.78	2.43

square-root metric. In the remaining part of this section, we demonstrate the data application using the Frobenius metric.

Specifically, we fitted the nonparametric CORE in (3.8) separately for the AD and CN subjects over different output points for age t and total cognitive score x . The bandwidths in the local fits for both the age and total cognitive score directions were chosen satisfying a leave-one-out cross validation criterion with a bivariate Gaussian kernel function, which led to the bandwidths in Table 3.

We fitted the proposed model at the $x = 10\%$, 50% , and 90% quantile values in the total cognitive score direction where higher total score means larger cognitive impairment, each for a fixed level of $t = 10\%$, 50% , and 90% in the age direction. We find that, given a quantile value t as the output point in the age direction, for higher scores and thus increased cognitive impairment, the overall magnitude of the absolute values of the pairwise correlations are smaller, and interestingly there are fewer negative correlations. These effects are more pronounced at older age.

Perhaps the most interesting finding from the fit (Figure 4) is the variation of Negative Functional Connectivity (NFC) for the AD subjects [71, 8, 63]. The positive pairwise correlations between the functional hubs, though reduced in magnitude, have a higher count when moving from a lower to a higher value in the total cognitive score direction. However, in the same context, the negative correlations diminish much more ostensibly in number and magnitude. Thus an increasing reduction in the negative connectivity can be associated with higher cognitive impairment, and hence an increased cognitive impairment, in the AD subjects. Diagnostic plots and visualizations for the fitted nonparametric CORE model for the AD subjects are provided in Appendix A.

The association between the functional connectivity and total cognitive score is modulated by age, in the sense that at lower ages the association between cognitive impairment and reduction in Negative Functional Connectivity is weaker than it is at higher ages. Table 4 shows the total magnitude of the correlations present in the estimated matrices, measured from the fits in Figure 4. The differences between the total magnitude of the positive and the negative pairwise correlations, the latter being subtracted from the former, is also shown in the table. We note that the total magnitude of the pairwise correlations present between the seed voxels diminishes with an increased value of the total cognitive score x and age t . This suggests weakened connectivity correlation, and thus a higher cognitive deficit, associated with a larger value of the cognitive score and higher age among AD subjects. The differences between the magnitudes of the total positive and negative correlations increase steadily, as the effect (number and magnitude) of negative correlations fades away faster with higher age and

TABLE 4

Each entry in the upper panel of the table shows respectively, the total magnitude of the positive plus negative correlation values, while each entry in the lower panel shows the difference in the total magnitudes of the overall positive correlations and the overall negative correlations present in the estimated matrices in Figure 4 at varying output points of total cognitive score and age. The lower, median, and higher levels are 10%, 50%, and 90% quantiles, respectively, for both the total cognitive score and the age directions.

	Lower Score	Median Score	Higher Score
Lower Age	9.20	4.99	5.97
Median Age	4.07	3.11	4.43
Higher Age	3.47	4.00	2.62
	Lower Score	Median Score	Higher Score
Lower Age	0.54	0.74	0.94
Median Age	0.92	1.47	1.76
Higher Age	1.55	1.42	1.77

higher values of the total cognitive score. A similar concurrent or time-varying pattern in the estimated correlation matrices is also present for the CN subjects (Figure 17 in the Appendix E).

The CORE model can be used to estimate the time-varying nature of the mean functions, and in this data illustration it captures how the pairwise connectivity correlation between any two seed voxels in the brain is changing over age. The dynamics of the connection is shown against age for the AD and CN subjects in Figure 5. Six pairs of voxels are chosen, which show the most change in magnitude of the pairwise correlation in Figure 4, and the nonparametric CORE model fitted at $x = 10\%$, 50% , and 90% quantiles of the total cognitive score, respectively, for varying ages for the AD and CN subjects separately. We observe that for the AD subjects (in red) the pairwise correlations between the chosen seed voxels get generally weaker with increasing age as both the positive and negative functional correlations tend to diminish in magnitude. Further, the (dotted) lines corresponding to the higher value of the total cognitive score result in weaker correlations over age. This pattern is not so discernible for the CN subjects (in green) for the chosen seed voxels.

We also fitted the partially global CORE, as defined in (4.1), to the same data and compared their performance, where the effect of total cognitive scores on the age-dependent functional connectivity correlation matrices is modeled as linear and the effect of age as nonparametric. To this end, the model was fitted separately for the AD and the CN subjects. The bandwidth parameter in the “age” direction was again chosen using a leave-one-out cross validation criterion and a Gaussian kernel was used. For the AD and CN subjects the optimal bandwidths were found to be 4.12 and 3.22, respectively. We present the fits corresponding to the AD subjects over a range of output points in Figure 6. We find a similar pattern for the fitted correlation. The overall magnitude of pairwise correlations diminish with age, however, the change is not so clear in the score direction. This could be attributed to the nonlinear, possibly quadratic trend in the cognitive score values (see Figure 6 and Figure 13 in Appendix A), that the linear weights of the partially global model do not reflect quite well.

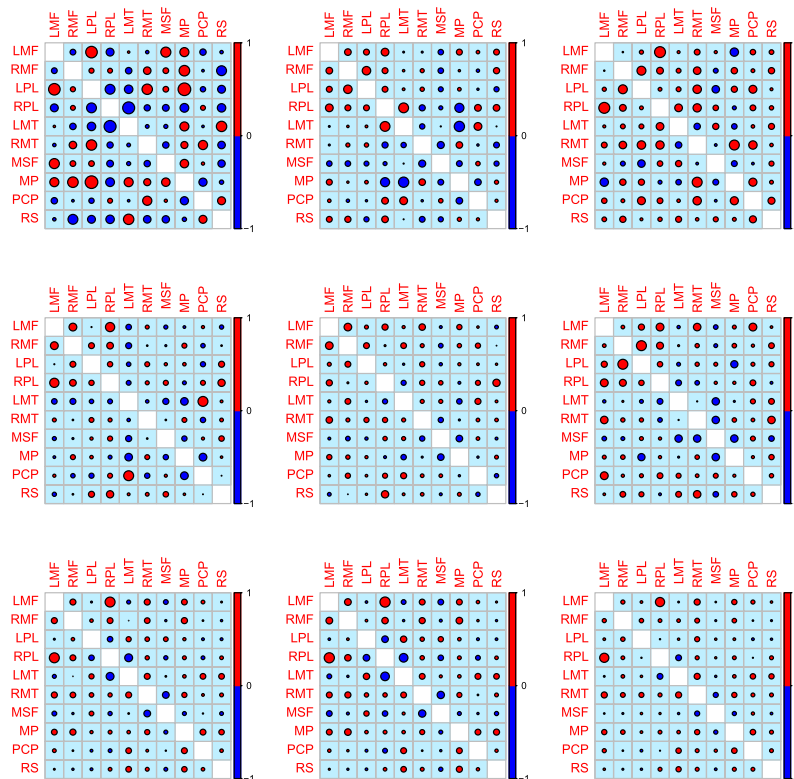


FIG 4. Estimated correlation matrix for the AD subjects fitted locally using nonparametric CORE in (3.8). The top, middle and bottom rows show, respectively, the fitted correlation matrices at 10%, 50%, and 90% quantiles of age. For each such age quantile, the columns (from left to right) depict the estimated correlation structure at $x = 10\%$, 50% , and 90% quantiles of total cognitive score respectively. Positive (negative) values are drawn in red (blue) and larger circles correspond to larger absolute values. The figure illustrates the dependence of functional connectivity on total cognitive score, modulated by age.

The Negative Functional Correlations seem to diminish in effect with higher age and total cognitive score values.

To investigate the comparative goodness-of-fit of the two models, we computed the average deviation of the fitted from the observed correlation matrices over the age interval $[55, 90]$,

$$\text{MSE}_{\oplus}(t) := d_F^2(M_{\oplus}(t), \hat{M}_{\oplus}(t)), \quad (6.2)$$

$M_{\oplus}(t)$ and $\hat{M}_{\oplus}(t)$ being the observed and fitted connectivity matrices, respectively, at age $t \in [55, 90]$ and $d_F(\cdot, \cdot)$ the Frobenius distance between two correlation matrices. Deviation (6.2) is displayed in Figure 7 for both the nonparametric and partially global CORE models. The partially global model seems to fit the data better, which could indicate that the linear constraint for the impact of

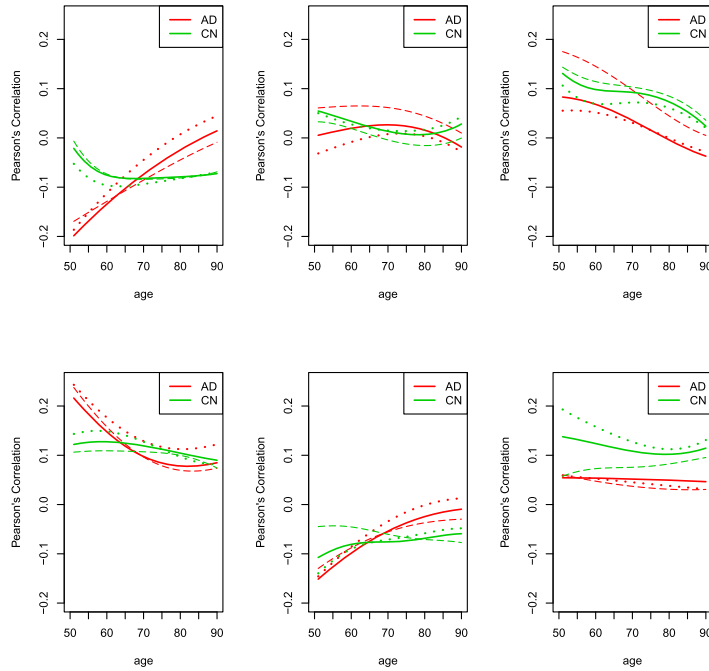


FIG 5. Figure showing the time (age)-varying nature of the fitted inter-hub pairwise correlations for six chosen connectivity hubs (RMF-MSF, RMF-PCP, RMF-RS, RMT-MP, MSF-RS, and PCP-RS, clockwise in the six panels, starting at upper left) for the AD and CN subjects. The dashed, solid, and dotted lines represent the estimated correlation at $x = 10\%$, 50% , and 90% quantiles of the total cognitive score, respectively, for varying ages. For the AD subjects, the positive (negative) correlations tend to decrease (increase) towards zero with increasing age. This pattern is not very evident for the CN subjects.

total cognitive score imposed in the partially global CORE model is likely satisfied. The integrated deviance $\int_{\mathcal{T}} \text{MSE}_{\oplus}(t) dt$ is 0.0570 for the nonparametric CORE and 0.0494 for the Partially CORE.

We further look into the out-of-sample prediction performance of the two methods for the AD subjects and CN subjects separately. For this, we first randomly split the dataset into a training set with sample size n_{train} and a test set with the remaining n_{test} subjects. We then take the fitted objects obtained from the training set, and predict the responses in the test set using the covariates present in the test set. As a measure of the efficacy of the fitted model, we compute root mean squared prediction error as

$$\text{RMPE} = \left[\frac{1}{n_{\text{test}}} \sum_{i=1}^{n_{\text{test}}} n_i^{-1} \sum_{l=1}^{n_i} d_F^2 \left(Y_{il}^{\text{test}}, \hat{l}_{\oplus}(X_{il}, T_{il}) \right) \right]^{-1/2}, \quad (6.3)$$

where Y_{il}^{test} and $\hat{l}_{\oplus}(X_{il}, T_{il})$ denote, respectively, the i^{th} actual and predicted responses in the test set, evaluated at age T_{il} and total cognitive score X_{il} . We

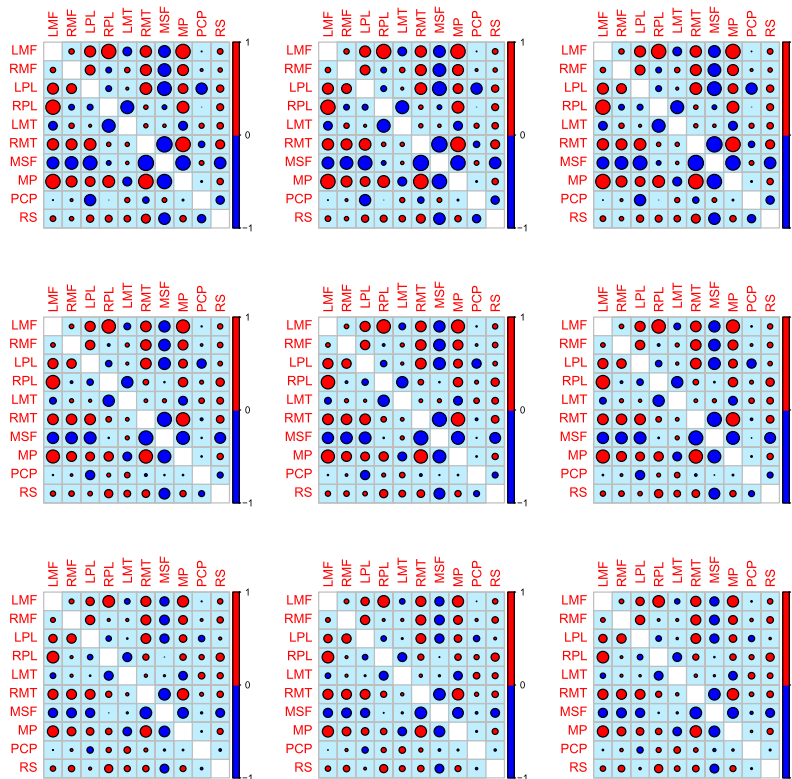


FIG 6. Estimated correlation matrix for the AD subjects fitted locally using partially global CORE in (4.1). The top, middle and bottom rows show, respectively, the fitted correlation matrices at 10%, 50%, and 90% quantiles of age. For each such age quantile, the columns (from left to right) depict the estimated correlation structure at $x = 10\%$, 50% , and 90% quantiles of total cognitive score respectively. Positive (negative) values are drawn in red (blue) and larger circles correspond to larger absolute values. The figure illustrates the dependence of functional connectivity on total cognitive score, modulated by age.

repeat this process 1000 times, and compute RMPE for each split for the AD and CN subjects separately (See Table 5).

TABLE 5
Average Root Mean Prediction Error (RMPE) over 1000 repetitions for the AD and CN subjects, as obtained from the local fits of the nonparametric and partially global CORE models. Here, n_{train} and n_{test} denote the sample sizes for the split training and testing datasets respectively.

	n_{train}	n_{test}	nonparametric CORE	partially global CORE)
AD	52	26	0.306	0.322
CN	271	100	0.151	0.167

We observe that the out-of-sample predictions errors are quite low for both the AD and CN subjects. In fact they are in the ballpark of the in-sample-

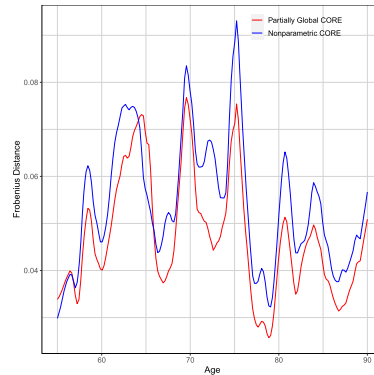


FIG 7. Comparison of fits for the two CORE models. The figure shows the average Frobenius distances between the fitted and the observed correlation matrices across age for the AD subjects using the nonparametric CORE model (blue) and the partially global CORE model (red) are illustrated.

prediction error, calculated as the average distance between the observed training sample and the predicted objects based on the covariates in the training sets, which supports the proposed CORE models. The nonparametric model shows a better predictive performance than the partially global CORE.

To confirm the group differences in the time-varying structure of the correlation matrices we further conduct a permutation test. To test the null hypothesis that, for varying age and total cognitive score values, the AD and CN subjects have the same conditional correlation matrix objects, we use the heuristic test statistic, measuring the average discrepancy of the fit for the AD and CN groups as

$$\int S(x, t) dx dt = \int d_F^2 \left(\hat{\Sigma}^{\text{AD}}(x, t), \hat{\Sigma}^{\text{CN}}(x, t) \right) dx dt. \quad (6.4)$$

Here $\hat{\Sigma}^{\text{AD}}(x, t)$ and $\hat{\Sigma}^{\text{CN}}(x, t)$ denote the estimated correlation matrix objects at total cognitive score x and age t , for the AD and CN subjects respectively, with $x \in [5, 70]$ and varying age $t \in [55, 90]$ and $d_F(\cdot, \cdot)$ is the Frobenius norm between two matrix objects.

All the observations are pooled, and the test statistic calculated for every possible way of dividing the pooled values into two groups of size 174 and 694. The set of these calculated test statistic values is the exact distribution of possible differences under the null hypothesis. The p-value of the test is calculated as the proportion of sampled permutations where the computed test-statistic value is more than or equal to the test statistic value obtained from the observed sample. Using 10^6 permutation samples, and the estimation methods being the nonparametric CORE and partially global CORE, the p-values are found to be 0.009 and 0.002, respectively. Thus both the methods are able to detect a significant difference in the functional connectivity between the AD and CN subjects, providing evidence that the CORE model is useful to differentiate

these groups. A further look into the time-varying regression fits for those connectivity hubs that show a change in the magnitude of the correlations across the AD and CN subjects (see Figure 5) also indicates differences between the AD and CN subjects.

6.2. Impact of GDP on human mortality

The Human Mortality Database (<https://www.mortality.org/>) provides yearly life table data differentiated by gender for 37 countries across 50 years. For our analysis, we considered the life tables for males according to yearly age-groups varying from age 0 to 120 for 22 countries over 14 calendar years, 1997-2010. Life tables can be viewed as histograms, which then can be smoothed with local least squares to obtain smooth estimated probability density functions for age at death. We carried this out for each year and country, using the Hades package available at <https://stat.ucdavis.edu/hades/> for smoothing the histograms with a choice of the bandwidth as 2 to obtain the age-at-death densities. Thus these data can be viewed as a sample of time-varying univariate probability distributions, for a sample of 22 countries, where the time axis represents 14 calendar years and the observations made at each calendar year for each country correspond to the age at death distribution, over the age interval $[0, 120]$, for that year. An illustration of the time-varying age at death distributions represented as density functions over the calendar years for four selected countries is in Figure 19 in the Appendix E.

The data on GDP per capita at current prices is available at the World Bank Database at <https://data.worldbank.org>. Considering the observed age-at-death densities for the countries over the calendar years as time-varying random objects that reside in the space of distributions equipped with the Wasserstein-2 metric, and GDP per capita for these countries as real-valued time-varying covariates, we fit the proposed concurrent object regression (CORE) models as described in Section 3 and 4. Figure 8 illustrates the time-varying nature of the fitted nonparametric CORE model, as per (3.8). We observe that for a fixed calendar year t the fitted densities appear to shift towards the right as the value of the covariate GDP increases, thus indicating that GDP per capita is positively associated with longevity at a fixed calendar year. If alternatively moving along the calendar years for a fixed GDP-value, one again observes an increasing trend in longevity.

Figure 9 shows the 3D plots for the fitted densities over the years for four countries- Australia, Finland, Portugal and the USA. We find that over the calendar years the modes for the age-at-death densities are shifted towards older age and that the probability of death before age 5 declines for all the four countries, indicating increasing life expectancy. Also, we notice that, for example, the USA improves on child mortality over the years while for Finland it remains low throughout. These fits match quite well with the observed densities in Figure 19 (see the Appendix E).

Further, the time-varying nature of the observed and estimated age-at-death densities are illustrated in Figure 10 and 11 for the USA. The left and right

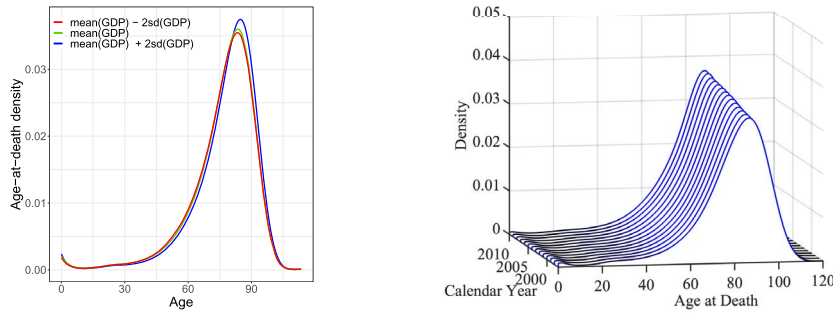


FIG 8. *Fitting the nonparametric concurrent object regression (CORE) model in (3.8). In the left panel, the locally fitted densities of human mortality distributions, at the year $t = 2005$ and GDP value $x = \text{mean}(GDP) - 2 \times \text{sd}(GDP)$, $x = \text{mean}(GDP)$ and $x = \text{mean}(GDP) + 2 \times \text{sd}(GDP)$ are displayed in red, green and blue lines respectively. The right panel shows the fitted densities for the USA, varying over the years 1997-2010.*

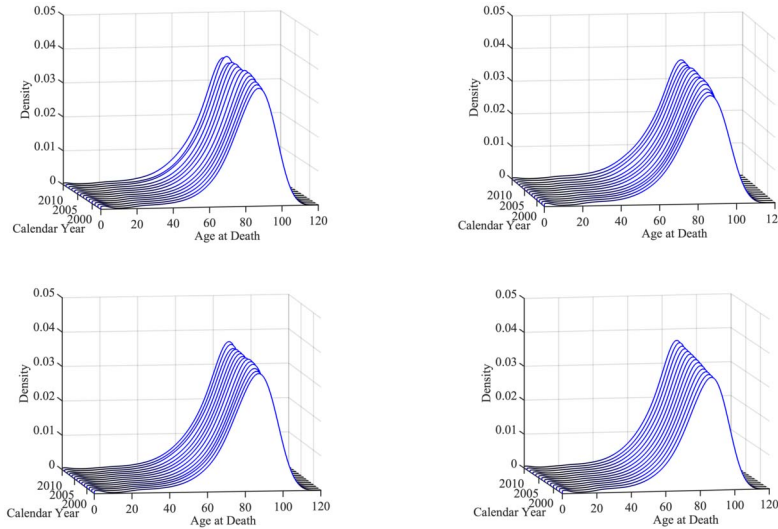


FIG 9. *Estimated age at death density functions over the years for males in Australia, Finland, the USA, and Portugal, clockwise in the four panels, starting at the upper left.*

panels of Figure 10 show the observed and estimated densities over the years. The nonparametric concurrent regression (CORE) model provides reasonable estimates of the observed densities and is able to recover a pattern of longevity extension in that the modes of the densities are shifting rightwards with increasing calendar time, thus indicating increasingly later age-at-death as expected. This observation is in line with the heatmap contours for the estimated distributions over the years for the USA, which is displayed in Figure 11, with calendar year as the Y-axis and the estimated age-at-death densities as the X-

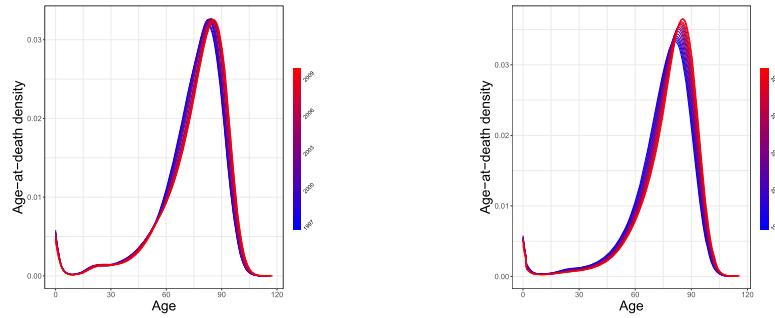


FIG 10. The left and right panel of the figure show the observed and estimated age-at-death densities over the years for males in the USA, respectively.

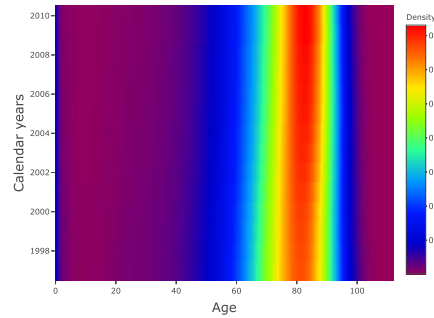


FIG 11. Figure displaying the heatmap contours for the estimated density functions over the years.

axis, linearly interpolating between years for continuity. The variation from year to year is marked by an increase in both the location and height of the peak in mortality. We also fitted the partially global CORE, as defined in (4.1), to the same data and compared their performance, where the effect of GDP is modeled as linear and the effect of calendar year as nonparametric. The left panel of Figure 12 indicates that the fits are very similar at randomly chosen points $x = \text{mean}(\text{GDP}); t = 2005$.

For both models, the bandwidth h is chosen by leave-one-out cross validation method, as the minimizer of the mean discrepancy between the regression estimates and the observed age-at-death density functions and a Gaussian kernel is used. To investigate the comparative goodness-of-fit of the two models further, we computed the average deviation of the fitted from the observed densities for each of the 14 calendar years as

$$\text{MSE}_{\oplus}(t) := \frac{1}{n} \sum_{i=1}^n d_W(f_{i\oplus}(t), \hat{f}_{i\oplus}(t)), \quad (6.5)$$

$f_{i\oplus}(t)$ and $\hat{f}_{i\oplus}(t)$ being the observed and fitted age-at-death densities for the

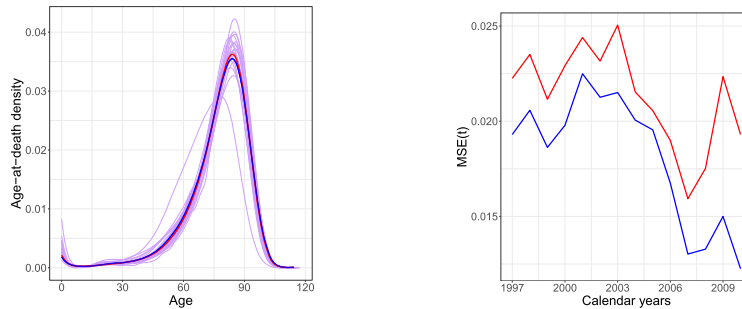


FIG 12. Comparing the fits of partially global (4.1) and nonparametric (3.8) concurrent object regression (CORE) models. The left panel shows the local fits at the points $x = \text{median}(X)$, $t = 2005$, comparing both models. The blue and red curves represent the nonparametric and the partially global regression fits, respectively. The purple curves in are the observed densities for the year 2005. In the right panel the average Wasserstein distances between the fitted and the observed densities across the calendar years for the nonparametric model (blue) and the partially global model (red) are illustrated.

i^{th} country, $i = 1, \dots, n$, respectively, at calendar years $t \in \{1997, \dots, 2010\}$ and $d_W(\cdot, \cdot)$ the Wasserstein-2 distance between two densities (distributions). Deviation (6.5) is displayed in the right panel of Figure 12 for both the nonparametric and partially global CORE models. The nonparametric model seems to fit the data better, which could indicate that the linear constraint for the impact of GDP imposed in the partially global Core model is likely not satisfied. The integrated deviance $\int_{\mathcal{T}} \text{MSE}_{\oplus}(t) dt$ is 0.413 for the nonparametric CORE and 0.580 for the Partially CORE.

Observe that there is big outlier in Figure 12 in the observed age-at-death densities for the country Bulgaria. This might have a large leverage or influence in the GDP per capita vs mortality regression relationship. We carry out the same analysis after removing this possible outlier (see Appendix C).

7. Concluding remarks

The proposed concurrent object regression (CORE) is useful for the regression analysis of random objects, where it complements Fréchet regression, by extending the notion of conditional Fréchet means further to a concurrent or varying coefficient framework. We provide theoretical justifications including rates of pointwise convergence for both global and local versions of the CORE model, and a uniform convergence result for the global part. For the special case of Euclidean objects the rates of convergence correspond to the known optimal rates. The rate of convergence for the nonparametric CORE model is intrinsically connected to an inherent manifold structure of the predictor space. Analogously to local regression, the nonparametric estimators will suffer from the curse of dimensionality if the predictor space is of higher dimension than $p = 2$ or $p = 3$. This calls for future research in dimension reduction in the predictor space. A

feature of interest is that we do not require observing the complete stochastic processes $\{(X(t), Y(t)) : t \in \mathcal{T}\}$ but only need samples taken at random predictor times, and our methods can be adapted for sparse and longitudinal predictors.

Appendix A: Model diagnostic plots for ADNI data application in Section 6.1

We illustrate the visualization of our fitted model and run diagnostic plots to gain insights into how the CORE models fit the data. For the ADNI data application in Section 6.1, the responses are random correlation matrix objects, residing in the space of positive semi-definite matrices equipped with the Frobenius norm. Thus data visualization and model diagnostic is a challenging and very important tool for regression of such random objects, as the regression relation may be even more difficult to discern among the complex details of the objects.

We define an analogue of squared residuals from the estimation as $r_{il}^2 = d_F^2(Y_{il}, \hat{Y}_{il})$, where Y_{il} and \hat{Y}_{il} are the observed and estimated correlation matrices for $i = 1, \dots, n$, and $l = 1, \dots, n_i$, and d_F is the Frobenius norm. Note that the squared residual distances are always positive, just like for the Euclidean case. Heuristically by plotting the squared residuals r_{il}^2 s against the “predicted” distances $d_F^2(\hat{\mu}_F, \hat{Y}_{il})$, the one can discern patterns to associate with a lack of fit of the model (see the left panel of Figure 13). Here the predicted distances measure the distance of each fitted observation \hat{Y}_{il} from their empirical barycenter $\hat{\mu}_F = \operatorname{argmin}_{\omega \in \Omega} \frac{1}{n} \sum_{i=1}^n \frac{1}{n_i} \sum_{l=1}^{n_i} d^2(\hat{Y}_{il}, \omega)$ as a baseline. More points are concentrated towards a smaller value for the distance in the x -axis suggesting that the fitted observations are mostly close to their their empirical barycenter. A lack of pattern in the figure shows a good fit for the model. The right panel of Figure 13 shows the scatter plot for the data pairs $(X_i(T_{il}), T_{il})$ in the predictor space, as a part of the process. We notice a quadratic trend for the increase in the total cognitive score X with age T . To this end, we fit a local linear model to get an estimate of $X(T)$ vs T in the predictor space.

Appendix B: ADNI data application in Section 6.1 using square root power metric

In this section we consider the space of positive semi definite matrices equipped with the square-root power metric. Let $S = U\Lambda U^T$ be the usual spectral decomposition with U an orthogonal matrix and Λ diagonal with strictly positive entries. A broad family of covariance matrix metrics is the set of power Euclidean metrics

$$d_A(S_1, S_2) = \|S_1^\alpha - S_2^\alpha\|_F, \quad \alpha \geq 0. \quad (\text{B.1})$$

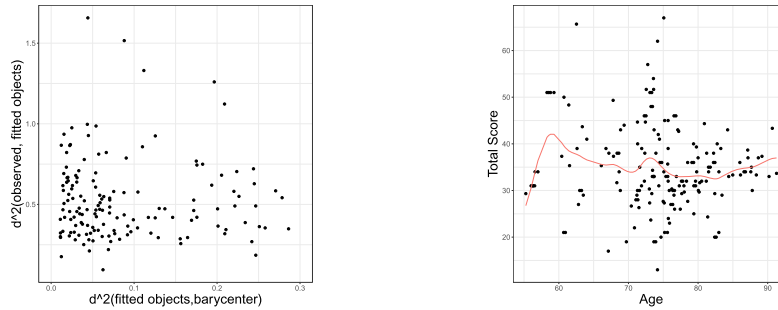


FIG 13. Visualization of the model diagnostics for the nonparametric concurrent object regression (CORE) model in (3.8) for AD subjects. The left panel shows the residual-vs-fitted distance plots. In the right panel the plot of $X(T)$ vs T is shown along with a local linear fit in red.

where $S_j^\alpha = U_j \Lambda_j^\alpha U_j^T$ for some orthogonal matrix U_j and diagonal matrix with strictly positive entries Λ_j for $j = 1, 2$ and $\|S\|_F = \sqrt{\text{trace}(X^T X)}$ is the Frobenius norm. We may consider any $\alpha \in \mathbb{R}$ depending on the specific situation. The special cases of $\alpha = 0$ corresponds to the log-Euclidean metric [17] while $\alpha = 1$ is just the Frobenius distance.

For many useful application $\alpha = 1/2$ is chosen [56, 46, 53] as a suitable metric. Figure 14 below is an analog of Figure 4 in Section 6.1, where the nonparametric CORE model in (3.8) is fitted over different output points for age t and total cognitive score x for the AD (Alzheimer's) subjects. The time-varying or concurrent regression framework is carried out with the Pearson correlation matrices in (6.1) as time-varying object responses, residing in the metric space of positive semi-definite matrices equipped with the square-root power norm, and total cognitive scores as real-valued covariates, changing with time (age in years). As before, the bandwidths in the local fits for both the age and total cognitive score directions were chosen satisfying a leave-one-out cross validation criterion with a bivariate Gaussian kernel function.

The proposed model is fitted at the $x = 10\%$, 50% , and 90% quantile values in the total cognitive score direction, where higher total score means larger cognitive impairment, each for a fixed level of $t = 10\%$, 50% , and 90% in the age direction. Our finding is similar to that in Figure 4. We find that for AD subjects an overall smaller magnitude of the absolute values of the pairwise correlations can be associated with higher total cognitive scores and thus increased cognitive impairment, the effects being more pronounced at older age.

Appendix C: Mortality-vs-GDP data application in Section 6.2 after removing outlier observation

The country Bulgaria seems to be an outlier among the sample of age-at-death densities for different countries over the years and has a right-skewed distribution. We rerun the data analysis after removing Bulgaria from the sample.

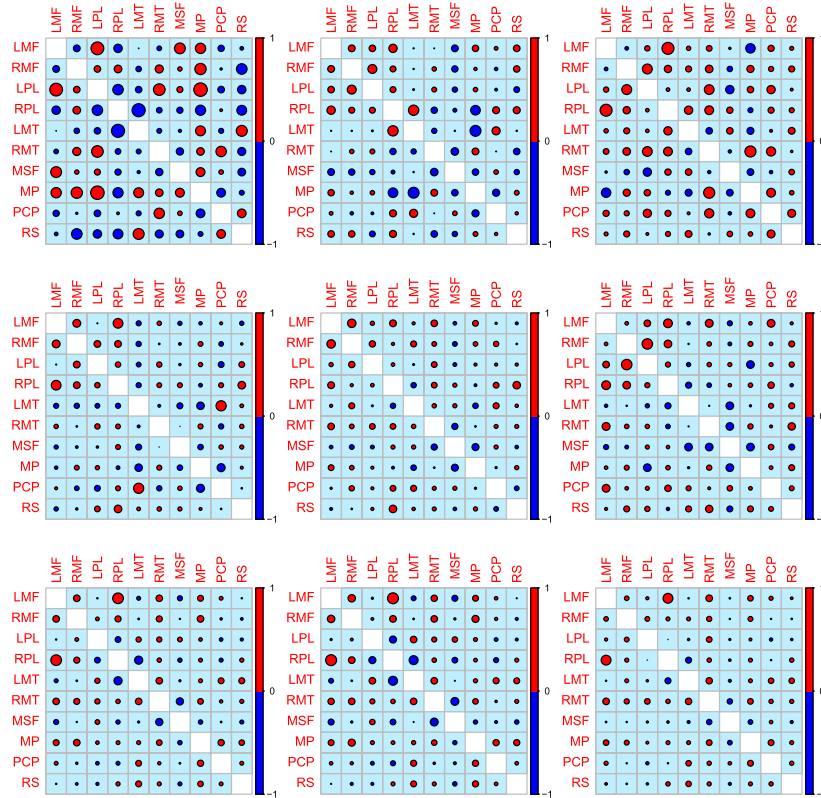


FIG 14. Estimated correlation matrix for the AD subjects fitted locally by nonparametric CORE in (3.8) using the square-root power metric. The top, middle and bottom rows show, respectively, the fitted correlation matrices at 10%, 50%, and 90% quantiles of age. For each such age quantile, the columns (from left to right) depict the estimated correlation structure at $x = 10\%$, 50% , and 90% quantiles of total cognitive score respectively. Positive (negative) values are drawn in red (blue) and larger circles correspond to larger absolute values. The figure illustrates the dependence of functional connectivity on total cognitive score, modulated by age.

In the left panel of Figure 15, the nonparametric and partially global concurrent object regression models are fitted at chosen points ($x = \text{median}(\text{GDP})$, $t = 2005$), while the right panel of Figure 15 shows the comparative goodness-of-fit of the two CORE models by computing the average deviation of the fitted from the observed densities for each of the 14 calendar years from 1997 to 2010 as per equation (6.5). After removing the possible outlier from the sample, the performances of the partially global nonparametric CORE models look very similar.

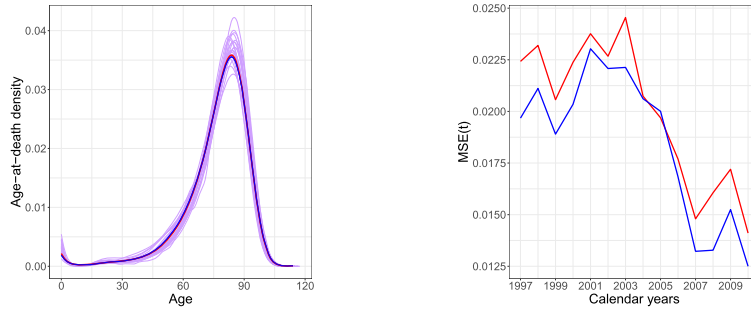


FIG 15. Comparing the fits of partially global (4.1) and nonparametric (3.8) concurrent object regression (CORE) models after removing the outlier from the sample. The left panel shows the local fits at the points $x = \text{median}(X)$, $t = 2005$, comparing both models. The blue and red curves represent the nonparametric and the partially global regression fits, respectively. The purple curves in the left panel are the observed densities for the year 2005. In the right panel the average Wasserstein distances between the fitted and the observed densities across the calendar years for the nonparametric model (blue) and the partially global model (red) are illustrated.

Appendix D: Technical proofs and additional lemmas

D.1. Proofs for Section 3

Recall the definition of the auxiliary parameters introduced in (3.4),

$$\mu_{jk} = E(K_{h_1, h_2}(X - x, T - t)(X - x)^j(T - t)^k), \text{ and}$$

$$\tau_{jk}(y) := E(K_{h_1, h_2}(X - x, T - t)(X - x)^j(T - t)^k | Y = y) \text{ for all } j, k = 0, 1, 2.$$

Lemma D.1. Under assumptions (A1), (A2),

$$\begin{aligned} \mu_{jk} &= h^{j+k} \left[f_{X,T}(x, t) K_{jk} + h K_{(j+1)k} \left(\frac{\partial}{\partial z} f_{X,T}(z, s) \right) \Big|_{(x,t)} \right. \\ &\quad \left. + h K_{j(k+1)} \left(\frac{\partial}{\partial s} f_{X,T}(z, s) \right) \Big|_{(x,t)} + O(h^2) \right], \\ \tau_{jk}(y) &= h^{j+k} \left[f_{(X,T)|Y}(x, t, y) K_{jk} + h K_{(j+1)k} \left(\frac{\partial}{\partial x} f_{(X,T)|Y}(z, s, y) \right) \Big|_{(x,t)} \right. \\ &\quad \left. + h K_{j(k+1)} \left(\frac{\partial}{\partial t} f_{(X,T)|Y}(z, s, y) \right) \Big|_{(x,t)} + O(h^2) \right], \end{aligned}$$

where the $O(h^2)$ terms are uniform over $y \in \Omega$.

Proof. It is a straightforward application of a Taylor expansion around the neighborhood of the point (x, t) on the densities, making use of the assumptions. □

Recall,

$$\sigma_0^2 = (\mu_{00}\mu_{20}\mu_{02} - \mu_{00}\mu_{11}^2 - \mu_{10}^2\mu_{02} - \mu_{01}^2\mu_{20} + 2\mu_{01}\mu_{10}\mu_{11}).$$

From Lemma D.1, it follows that $\sigma_0^2 = h^4 [M f_{X,T}^3(x, t) + O(h)]$ for some constant $M > 0$.

Lemma D.2. *Under assumptions (A1)-(A7) and additionally assuming that,*
 $\sup_{x,t,y} |f''_{(X,T)|Y=y}(x, t, y)| < \infty,$

$$\tilde{L}_\oplus(\omega, x, t) = M_\oplus(\omega, x, t) + O(h^2).$$

Proof. The proof follows a similar line of argument as in the proof of Theorem 3 in [44] with some necessary changes due to the differences in the setup. We first establish that

$$\frac{dF_{Y|(X,T)}(y, x, t)}{dF_Y(y)} = \frac{f_{(X,T)|Y}(x, t, y)}{f_{(X,T)}(x, t)} \text{ for all } (x, t) \text{ such that } f_{X,T}(x, t) > 0. \quad (\text{D.1})$$

For any open set $U \subset \Omega$ define,

$$a(x, t) := \int_U \frac{f_{(X,T)|Y}(x, t, y)}{f_{(X,T)}(x, t)} dF_Y(y); \quad b(x, t) = \int_U dF_{Y|(X,T)}(y, x, t),$$

and observe that by assumption (A3), both $a(\cdot, \cdot)$ and $b(\cdot, \cdot)$ are continuous functions of (x, t) . Then for any measurable set A in the Borel sigma algebra on \mathbb{R}^2 ,

$$\begin{aligned} \int_A a(x, t) f_{(X,T)}(x, t) dx dt &= \int_U \left(\int_A f_{(X,T)|Y}(x, t, y) dx dt \right) dF_Y(y) \\ &= \int_A \left(\int_U dF_{Y|(X,T)}(y, x, t) \right) f_{(X,T)}(x, t) dx dt = \int_A b(x, t) f_{(X,T)}(x, t) dx dt. \end{aligned}$$

The fact that this holds for any measurable set A then implies (D.1). Next observing that,

$$\begin{aligned} s^L(z, x, s, t, h_1, h_2) &= K_{h_1, h_2}(z - x, s - t) [\nu_1 + \nu_2(z - x) + \nu_3(s - t)] \\ &= \frac{1}{\sigma_0^2} K_{h_1, h_2}(z - x, s - t) \times \\ &\quad [(\mu_{20}\mu_{02} - \mu_{11}^2) + (\mu_{01}\mu_{11} - \mu_{02}\mu_{10})(z - x) + (\mu_{10}\mu_{11} - \mu_{20}\mu_{01})(s - t)] \end{aligned}$$

. we have, using Lemma D.1,

$$\begin{aligned} &\int s^L(z, x, s, t, h) dF_{(X,T)|Y}(z, s, y) \\ &= \frac{1}{\sigma_0^2} [(\mu_{20}\mu_{02} - \mu_{11}^2) \tau_{00}(y) + (\mu_{01}\mu_{11} - \mu_{02}\mu_{10}) \tau_{10}(y) \end{aligned}$$

$$\begin{aligned}
 & + (\mu_{10}\mu_{11} - \mu_{20}\mu_{01}) \tau_{01}(y)] \\
 & = \frac{f_{(X,T)|Y}(x, t, y)}{f_{(X,T)}(x, t)} + O(h^2),
 \end{aligned}$$

where the error term is uniform over $y \in \Omega$. Finally,

$$\begin{aligned}
 \tilde{L}_{\oplus}(\omega, x, t) & = \int d^2(y, \omega) s^L(z, x, s, t, h) dF(z, s, y) \\
 & = \int d^2(y, \omega) \left(\frac{f_{(X,T)|Y}(x, t, y)}{f_{(X,T)}(x, t)} + O(h^2) \right) dF_Y(y) \\
 & = \int d^2(y, \omega) \left(\frac{dF_{Y|(X,T)}(y, x, t)}{dF_Y(y)} + O(h^2) \right) dF_Y(y) \\
 & = \int d^2(y, \omega) dF_{Y|(X,T)}(y, x, t) + O(h^2) = M_{\oplus}(\omega, x, t) + O(h^2),
 \end{aligned}$$

where, again, the error term is uniform over $\omega \in \Omega$. Thus the intermediate objective function in (3.8) is a smoothed version of the true objective function in (2.1). \square

Proof of Proposition 3.1. Assumptions (A3), (A4) regarding the existence and uniqueness of the minimizer $\tilde{l}_{\oplus}(x, t)$ and the well-separateness of the objective functions at the minimizer imply $d(m_{\oplus}(x, t), \tilde{l}_{\oplus}(x, t)) = o(1)$ as $h = h_n \rightarrow 0$.

Next, similar to the proof of consistency of any M-estimator [58], we define $r_h = h^{-2}$ and set $S_{j,n} = \{\omega : 2^{j-1} < r_h d(\omega, m_{\oplus}(x, t)) \leq 2^j\}$. Denoting the indicator function by $\mathbf{1}(\cdot)$, for any large $M > 0$, under assumption (A5), there exists $a > 0$ such that, for large n ,

$$\mathbf{1}\left(r_h d(\tilde{l}_{\oplus}(x, t), m_{\oplus}(x, t)) > 2^M\right) \leq a \sum_{j \geq M} \frac{2^{-j}}{r_h^{-2} h^{-2}} \leq a \sum_{j \geq M} 2^{-j}.$$

The above series converges, yielding that for $M > 0$,

$$d(\tilde{l}_{\oplus}(x, t), m_{\oplus}(x, t)) \leq 2^M h^2 = O(h^2),$$

for large n . \square

Lemma D.3. *Under assumptions (A1), (A2), (A8), (A9),*

$$\hat{\mu}_{jk} = \mu_{jk} + O_p \left[(h^{2j+2k-1} n^{-1})^{\frac{1}{2}} \right].$$

Proof. We provide the proof for the case $p = 1$ only, that is when $X(t) \in \mathbb{R}$, for any $t \in \mathcal{T}$. The case $p > 1$ is based on essentially the same but more tedious arguments. The proof exploits the manifold structure of the predictor space as described before. The fact that $E(\hat{\mu}_{jk}) = \mu_{jk}$ follows immediately from the definitions. For calculating $\text{Var}(\hat{\mu}_{jk})$, first consider the case $n_i = 1$ for $i = 1, \dots, n$. For any given $t \in \mathcal{T}$ and $x = x(t) \in \mathbb{R}$, define

$$\Psi_{il} = K_h(X_{il} - x, T_{il} - t) (X_{il} - x)^j (T_{il} - t)^k. \tag{D.2}$$

Observe that

$$\begin{aligned}
& \text{Var}(\Psi_{il}) \leq E(\Psi_{il}^2) \\
& = E\left(K_h^2(X_{il} - x, T_{il} - t)(X_{il} - x)^{2j}(T_{il} - t)^{2k}\right) \\
& = E\left(K_h^2(X_{il} - x, T_{il} - t)(X_{il} - x)^{2j}(T_{il} - t)^{2k} \mathbf{1}\left((X_{il}, T_{il}) \in \mathcal{B}_h^{(2)}(x, t)\right)\right) \\
& \quad + E\left(K_h^2(X_{il} - x, T_{il} - t)(X_{il} - x)^j(T_{il} - t)^k \mathbf{1}\left((X_{il}, T_{il}) \notin \mathcal{B}_h^{(2)}(x, t)\right)\right) \\
& = \int \frac{1}{h^4} K^2\left(\frac{z-x}{h}, \frac{s-t}{h}\right) (z-x)^{2j} (s-t)^{2k} \times \\
& \quad \mathbf{1}\left((z, s) \in \mathcal{B}_h^{(2)}(x, t)\right) f_{(X,T)}(z, s) dz ds + O(h^{1+2j+2k}). \tag{D.3}
\end{aligned}$$

The last line follows from Assumption (A8). Now, since, for all $(z, s) \in \mathcal{B}_h^{(2)}(x, t)$, we have $|z-x| \leq h$ and $|s-t| \leq h$, it follows from (D.3) that

$$\begin{aligned}
& E(\Psi_{il}^2) \\
& \leq \int \frac{1}{h^4} K^2\left(\frac{z-x}{h}, \frac{s-t}{h}\right) h^{2j} h^{2k} \mathbf{1}\left((z, s) \in \mathcal{B}_h^{(2)}(x, t)\right) f_{(X,T)}(z, s) dz ds \\
& \quad + O(h^{1+2j+2k})
\end{aligned}$$

By change of variable, and using a second-order Taylor expansion of the two variable density function $f_{X,T}(\cdot, \cdot)$ around the given points (x, t) , the first term of the above can be simplified to

$$\begin{aligned}
& \int \frac{1}{h^4} K^2\left(\frac{z-x}{h}, \frac{s-t}{h}\right) h^{2j} h^{2k} \mathbf{1}\left((z, s) \in \mathcal{B}_h^{(2)}(x, t)\right) f_{(X,T)}(z, s) dz ds \\
& \leq h^{2j+2k-2} \int K^2(u, v) \mathbf{1}\left((u, v) \in \mathcal{B}_h^{(2)}(0, 0)\right) f_{(X,T)}(x+uh, t+vh) dudv \\
& = h^{2j+2k-2} \int K^2(u, v) \mathbf{1}\left((u, v) \in \mathcal{B}_h^{(2)}(0, 0)\right) \left[f_{X,T}(x, t) \right. \\
& \quad + uh \left(\frac{\partial}{\partial a} f_{X,T}(a, b) \Big|_{(x,t)} \right) + vh \left(\frac{\partial}{\partial b} f_{X,T}(a, b) \Big|_{(x,t)} \right) \\
& \quad + u^2 h^2 \left(\frac{\partial^2}{\partial a^2} f_{X,T}(a, b) \Big|_{(x_*, t_*)} \right) \\
& \quad \left. + v^2 h^2 \left(\frac{\partial^2}{\partial b^2} f_{X,T}(a, b) \Big|_{(x_*, t_*)} \right) + uv h^2 \left(\frac{\partial^2}{\partial a \partial b} f_{X,T}(a, b) \Big|_{(x_*, t_*)} \right) \right] dudv, \tag{D.4}
\end{aligned}$$

for some x_* between u and x , and some t_* between v and t . Now, using Cauchy-Schwartz inequality, and under assumption (A1), (A2), and (A9) it follows from (D.4) that

$$\int \frac{1}{h^4} K^2\left(\frac{z-x}{h}, \frac{s-t}{h}\right) h^{2j} h^{2k} \mathbf{1}\left((z, s) \in \mathcal{B}_h^{(2)}(x, t)\right) f_{(X,T)}(z, s) dz ds$$

$$\leq h^{2j+2k-2}[A_1h + A_2h^2 + A_3h^3] = O(h^{2j+2k-1}). \tag{D.5}$$

Combining (D.3) and (D.5) we have,

$$\text{Var}(\Psi_{il}) = O(h^{2j+2k-1}),$$

where the order term is independent of the index i and l . Now, note that the Ψ_{il} is independent across i . Thus

$$\text{Var}(\hat{\mu}_{jk}) = \text{Var}\left(\frac{1}{n} \sum_{i=1}^n \Psi_{il}\right) = \frac{1}{n^2} \sum_{i=1}^n \text{Var}(\Psi_{il}) = O(h^{2j+2k-1}n^{-1}).$$

For the case $n_i \geq 1$ we observe that the Ψ_{il} are not independent across l , as the covariates are measured $l = 1, \dots, n_i$ times for the same subject. However, Ψ_{il} are independent across $i = 1, \dots, n$. Using the result just derived for the case $n_i = 1$ and applying the Cauchy-Schwartz inequality,

$$\begin{aligned} \text{Var}(\hat{\mu}_{jk}) &= \text{Var}\left[\frac{1}{n} \sum_{i=1}^n \left(\frac{1}{n_i} \sum_{l=1}^{n_i} \Psi_{il}\right)\right] = \frac{1}{n^2} \sum_{i=1}^n \text{Var}\left(\frac{1}{n_i} \sum_{l=1}^{n_i} \Psi_{il}\right) \\ &= \frac{1}{n^2} \sum_{i=1}^n \left[\frac{1}{n_i^2} \sum_{l=1}^{n_i} \sum_{l'=1}^{n_i} \text{cov}(\Psi_{il}, \Psi_{il'})\right] \\ &\leq \frac{1}{n^2} \sum_{i=1}^n \left[\frac{1}{n_i^2} \sum_{l=1}^{n_i} \sum_{l'=1}^{n_i} \sqrt{\text{Var}(\Psi_{il})} \sqrt{\text{Var}(\Psi_{il'})}\right] \\ &= \frac{1}{n^2} \sum_{i=1}^n \left[\frac{1}{n_i^2} \sum_{l=1}^{n_i} \sum_{l'=1}^{n_i} O(h^{2j+2k-1})\right] = O(h^{2j+2k-1}n^{-1}). \end{aligned}$$

Since $E(\hat{\mu}_{jk}) = \mu_{jk}$ and $\text{Var}(\hat{\mu}_{jk}) = O(h^{2j+2k-1}n^{-1})$, the result follows using Chebyshev's inequality. \square

We note that Lemma D.3 also implies that $\hat{\sigma}_0^2 = O_P(n^{-\frac{1}{2}}h^{\frac{7}{2}})$ for the plug in estimator $\hat{\sigma}_0^2$ defined in (3.10).

Lemma D.4. Under assumptions (A1)- (A9), for any $t \in \mathcal{T}$ and $x = X(t)$,

$$d(\tilde{l}_{\oplus}(x, t), \hat{l}_{\oplus}(x, t)) = o_P(1).$$

Proof. We will first show that $\hat{L}_{\oplus} - \tilde{L}_{\oplus} \rightsquigarrow 0$ in $\ell^\infty(\Omega)$, where \rightsquigarrow denotes the weak convergence of a process and $\ell^\infty(\Omega)$ is the space of bounded functions on Ω . As a consequence of Theorem 1.3.6 of [58], this will imply that, $\|\hat{L}_{\oplus} - \tilde{L}_{\oplus}\|_{\Omega} := \sup_{\omega \in \Omega} |\hat{L}_{\oplus}(\omega) - \tilde{L}_{\oplus}(\omega)| \xrightarrow{\mathbb{P}} 0$, namely, the estimated objective function \hat{L}_{\oplus} in

(3.13) converges in probability to the intermediate objective function \tilde{L}_{\oplus} (2.1). The Lemma follows using Assumption (A4), recalling Theorem 3.2.3 of [58].

Define, $s_{il}^L := K_h(X_{il} - x, T_{il} - t) [\nu_1 + \nu_2(X_{il} + \nu_3(T_{il} - t))]$, where

$$\nu_1 = \frac{1}{\sigma_0^2} [\mu_{20}\mu_{02} - \mu_{11}^2],$$

$$\begin{aligned}\nu_2 &= \frac{1}{\sigma_0^2} [\mu_{01}\mu_{11} - \mu_{02}\mu_{10}], \\ \nu_3 &= \frac{1}{\sigma_0^2} [\mu_{10}\mu_{11} - \mu_{20}\mu_{01}], \\ \sigma_0^2 &= (\mu_{00}\mu_{20}\mu_{02} - \mu_{00}\mu_{11}^2 - \mu_{10}^2\mu_{02} - \mu_{01}^2\mu_{20} + 2\mu_{01}\mu_{10}\mu_{11}),\end{aligned}$$

and the definition of the auxiliary parameters μ_{jk} is given by the following, as described in (3.4)

$$\mu_{jk} = E(K_{h_1, h_2}(X - x, T - t)(X - x)^j(T - t)^k), \quad j, k = 0, 1, 2.$$

Then,

$$\begin{aligned}\hat{L}_\oplus(\omega) - \tilde{L}_\oplus(\omega) &= \frac{1}{n} \sum_{i=1}^n (n_i^{-1} \sum_{l=1}^{n_i} [s_{il}^L(x, t, h) - s_{il}^L(x, t, h)] d^2(Y_{il}, \omega)) \\ &+ \frac{1}{n} \sum_{i=1}^n (n_i^{-1} \sum_{l=1}^{n_i} [s_{il}^L(x, t, h) d^2(Y_{il}, \omega) - E(s_{il}^L(x, t, h) d^2(Y_{il}, \omega))]).\end{aligned}\quad (\text{D.6})$$

Observe that,

$$\hat{s}_{il}^L(x, t, h) - s_{il}^L(x, t, h) = K_h(X_{il} - x, T_{il} - t) [W_{1n} + W_{2n}(X_{il} - x) + W_{3n}(T_{il} - t)],$$

with

$$W_{1n} = \hat{\nu}_1 - \nu_1; \quad W_{2n} = \hat{\nu}_2 - \nu_2; \quad W_{3n} = \hat{\nu}_3 - \nu_3. \quad (\text{D.7})$$

Lemma D.1 and Lemma D.3 imply that $W_{1n} = O_P((nh)^{-1/2})$, $W_{2n} = O_P((nh^3)^{-1/2})$, $W_{3n} = O_P((nh^3)^{-1/2})$. Since

$$\begin{aligned}E(K_h(X_i(T_i) - x, T_i - t)(X_i(T_i) - x)^j(T_i - t)^k d^2(Y_i(T_i), \omega)) &= O(h^{j+k}), \\ E(K_h^2(X_i(T_i) - x, T_i - t)(X_i(T_i) - x)^{2j}(T_i - t)^{2k} d^4(Y_i(T_i), \omega)) &= O(h^{2j+2k-1}), \\ E(s_{il}^2(x, t, h)) &= O(h^{-1}),\end{aligned}$$

it follows that both terms in (D.6) are $O_P((nh)^{-1/2})$. Thus $\hat{L}_\oplus(\omega) - \tilde{L}_\oplus(\omega) = o_P(1)$ for any $\omega \in \Omega$. Also any finite dimensional distribution converges weakly, that is, for any k , $\hat{L}_\oplus(\omega_1) - \tilde{L}_\oplus(\omega_1), \dots, \hat{L}_\oplus(\omega_k) - \tilde{L}_\oplus(\omega_k) \rightsquigarrow 0$. This result along with the asymptotic equi-continuity of the process $(\hat{L}_\oplus(\omega) - \tilde{L}_\oplus(\omega))_{\omega \in \Omega}$ leads to the desired weak convergence of $(\hat{L}_\oplus - \tilde{L}_\oplus)_{\omega \in \Omega}$ in $\ell^\infty(\Omega)$. It remains to show that for any $\eta > 0$,

$$\limsup_N \mathbb{P} \left(\sup_{d(\omega_1, \omega_2) < \delta} \left| (\hat{L}_\oplus - \tilde{L}_\oplus)(\omega_1) - (\hat{L}_\oplus - \tilde{L}_\oplus)(\omega_2) \right| > \eta \right) \rightarrow 0 \text{ as } \delta \rightarrow 0.$$

For this we observe,

$$E(s_{il}^L(x, t, h)) = O(1); \quad E(s_{il}^2(x, t, h)) = O(h^{-1}),$$

$$\frac{1}{n} \sum_{i=1}^n n_i^{-1} \sum_{l=1}^{n_i} |\hat{s}_{il}^L(x, t, h)| = O_P(1),$$

yielding,

$$\begin{aligned} |\hat{L}_\oplus(\omega_1) - \hat{L}_\oplus(\omega_2)| &\leq 2 \operatorname{diam}(\Omega) d(\omega_1, \omega_2) \left[\frac{1}{n} \sum_{i=1}^n \left(\frac{1}{n_i} \sum_{l=1}^{n_i} |\hat{s}_{il}^L(x, t, h)| \right) \right] \\ &= O_P(d(\omega_1, \omega_2)), \text{ and} \\ |\tilde{L}_\oplus(\omega_1) - \tilde{L}_\oplus(\omega_2)| &\leq 2 \operatorname{diam}(\Omega) d(\omega_1, \omega_2) E(|s_{il}^L(x, t, h)|) = O(d(\omega_1, \omega_2)). \end{aligned}$$

Thus,

$$\begin{aligned} &\sup_{d(\omega_1, \omega_2) < \delta} \left| (\hat{L}_\oplus - \tilde{L}_\oplus)(\omega_1) - (\hat{L}_\oplus - \tilde{L}_\oplus)(\omega_2) \right| \\ &\leq \sup_{d(\omega_1, \omega_2) < \delta} \left| \hat{L}_\oplus(\omega_1) - \hat{L}_\oplus(\omega_2) \right| + \sup_{d(\omega_1, \omega_2) < \delta} \left| \tilde{L}_\oplus(\omega_1) - \tilde{L}_\oplus(\omega_2) \right| \leq \delta, \end{aligned}$$

which verifies asymptotic equi-continuity and hence the weak convergence of $(\hat{L}_\oplus(\omega) - \tilde{L}_\oplus(\omega))_{\omega \in \Omega}$ follows and also the result by assumption (A4). \square

Proof of Proposition 3.2. We follow a similar line of argument as in the proof of Theorem 4 in [44]. As before we define $s_{il}^L := s_{il}^L(x, t, h) = K_h(X_{il} - x, T_{il} - t) \times [\nu_1 + \nu_2(X_{il} + \nu_3(T_{il} - t))]$, and the difference between the estimated and intermediate objective functions are $T_n(\omega) = \hat{L}_\oplus(\omega, \cdot, \cdot) - \tilde{L}_\oplus(\omega, \cdot, \cdot)$ for any $\omega \in \Omega$. Also let $D_{il}(\omega, x, t) = d^2(Y_{il}, \omega) - d^2(Y_{il}, \tilde{l}_\oplus(x, t))$. We have

$$\begin{aligned} |T_n(\omega) - T_n(\tilde{l}_\oplus(x, t))| &\leq \left| \frac{1}{n} \sum_{i=1}^n \frac{1}{n_i} \sum_{l=1}^{n_i} [\hat{s}_{il}^L(x, t, h) - s_{il}^L(x, t, h)] D_{il}(\omega, x, t) \right| \\ &\quad + \left| \frac{1}{n} \sum_{i=1}^n \frac{1}{n_i} \sum_{l=1}^{n_i} [s_{il}^L(x, t, h) D_{il} - E(s_{il}^L D_{il})] \right| \quad (\text{D.8}) \end{aligned}$$

We have seen that from (D.7), $W_{1n} = O_P((nh)^{-1/2})$, $W_{2n} = O_P((nh^3)^{-1/2})$, $W_{3n} = O_P((nh^3)^{-1/2})$. Thus, noting that $|D_{il}(\omega, x, t)| \leq 2 \operatorname{diam}(\Omega) d(\omega, \tilde{l}_\oplus(x, t))$, the first term on the right hand side of (D.8) is $d(\omega, \tilde{l}_\oplus(x, t))$, where the order term is absolute, independent of ω and \tilde{l}_\oplus . Thus, we can define the set

$$\begin{aligned} B_R = & \left\{ \sup_{d(\omega, \tilde{l}_\oplus(x, t)) \leq \delta} \left| \frac{1}{n} \sum_{i=1}^n \frac{1}{n_i} \sum_{l=1}^{n_i} [\hat{s}_{il}^L(x, t, h) - s_{il}^L(x, t, h)] D_{il}(\omega, x, t) \right| \leq R\delta(nh)^{-1/2} \right\}, \quad (\text{D.9}) \end{aligned}$$

for $R > 0$ such that $P(B_R^c) \rightarrow 0$.

Next, to control the second term of the right hand side of (D.8), define the functions $g_\omega : \mathbb{R} \times \Omega \rightarrow \mathbb{R}$ such that

$$g_\omega(z, s, \omega) K_h(z - x, s - t) [\nu_1 + \nu_2(z - x) + \nu_3(s - t)] d^2(y, \omega),$$

and the corresponding function class

$$M_{n\delta} = \{g_\omega - g_{\tilde{l}_\oplus} : d(\omega, \tilde{l}_\oplus(x, t)) < \delta\}.$$

An envelope function for $M_{n\delta}$ is given by

$$G_{n\delta}(z, s) = 2 \operatorname{diam}(\Omega) \delta K_h(z - x, s - t) [\nu_1 + \nu_2(z - x) + \nu_3(s - t)],$$

such that $E(G_{n\delta}^2(z, s)) = O(\delta^2 h^{-1})$. Thus, using Theorems 2.7.11 and 2.14.2 of [58] together with Assumption (A3), we have, for small δ ,

$$\begin{aligned} E \left(\sup_{d(\omega, \tilde{l}_\oplus(x, t)) < \delta} \left| \frac{1}{n} \sum_{i=1}^n \frac{1}{n_i} \sum_{l=1}^{n_i} [s_{il}^L(x, t, h) D_{il}(x, t) - E(s_{il}^L(x, t, h) D_{il}(x, t))] \right| \right) \\ = O(\delta(nh)^{-1/2}). \end{aligned} \quad (\text{D.10})$$

Combining this in (D.8) and the definition of B_R in (D.9),

$$E \left(\mathbf{1}(B_R) \sup_{d(\omega, \tilde{l}_\oplus(x, t)) < \delta} |T_n(\omega) - T_n(\tilde{l}_\oplus(x, t))| \right) \leq a\delta(nh)^{-1/2},$$

where $\mathbf{1}(\cdot)$ denotes the indicator function and a is a constant depending on R and the entropy integral in (A7). To finish, let $r_n = (nh)^{1/2}$ and define $S_{j,n} = \{\omega : 2^{j-1} < r_n d(\omega, \tilde{l}_\oplus(x, t)) \leq 2^j\}$. Choose η_2 satisfying Assumption (A6) such that (A7) is satisfied for any $\delta < \eta_2$. Setting $\eta_* = \eta_2/2$ for any integer M ,

$$\begin{aligned} P \left(r_n d(\tilde{l}_\oplus(x, t), \hat{l}_\oplus(x, t)) > 2^M \right) &\leq P(B_R^c) + P(2d(\tilde{l}_\oplus(x, t), \hat{l}_\oplus(x, t)) > \eta_2) \\ &+ \sum_{j \geq M: 2^j \leq r_n \eta_*} P \left(\left\{ \sup_{\omega \in S_{j,n}} |T_n(\omega) - T_n(\tilde{l}_\oplus(x, t))| \geq C \frac{2^{2(j-1)}}{r_n^2} \right\} \cap B_R \right), \end{aligned} \quad (\text{D.11})$$

where the last term goes to zero for any $\eta_2 > 0$ by Lemma D.4. Since

$d(\omega, \tilde{l}_\oplus(x, t)) < 2^j/r_n$, on $S_{j,n}$, which implies that the sum on the right hand side of (D.11) is bounded by

$$4aC^{-1} \sum_{j \geq M: 2^j \leq r_n \eta_*} \frac{2^{-j}}{r_n^{-2}(nh)^{1/2}} \leq 4aC^{-1} \sum_{j \geq M} 2^{-j}.$$

The above series converges. Hence

$$d(\hat{l}_\oplus(x, t) = \tilde{l}_\oplus(x, t) = O_P(r_n) = O_P((nh)^{-1/2}). \quad \square$$

Theorem 3.1 is a consequence of combining Propositions 3.1 and 3.2 with a triangle inequality.

D.2. Background for the partially global concurrent object regression

Proof. Motivation of deriving (4.1) for the Euclidean response case. When $(\Omega, d) = (\mathbb{R}, d_E)$, we write $m_{\oplus}(\cdot, \cdot) = m(\cdot, \cdot)$. Assuming the true relation between the response Y and the predictor $X(T)$ is linear while there is a smooth non-parametric relation in the T direction, a partially local linear type estimator of the regression model $m(\cdot, \cdot)$ at the point $T = t$, $X(T) = x$ is given by $\hat{m}(x, t) = \hat{a}^T(x - \mu_X(t)) + \hat{\beta}_0$, where $\mu_X(t) = E(X|T = t) = E_{X|T=t}(X(t))$ for all $t \in \mathcal{T}$. This can be written alternatively as

$$(\hat{a}, \hat{\beta}_0, \hat{\beta}_1) = \underset{a, \beta_0, \beta_1}{\operatorname{argmin}} \frac{1}{n} \sum_{i=1}^n \left[\frac{1}{n_i} \sum_{l=1}^{n_i} K_h(T_{il} - t)(Y_{il} - a^T(X_{il} - \mu_X(t)) - \beta_0 - \beta_1(T_{il} - t))^2 \right].$$

We can view this as an M-estimator of an intermediate population model,

$$\tilde{g}(x, t) = (a_1^*(x, t))^T(x - \mu_X(t)) + \beta_0^*(t), \text{ where}$$

$$\begin{aligned} & (a_1^*, \beta_0^*, \beta_1^*) \\ &= \underset{a_1, \beta_0, \beta_1}{\operatorname{argmin}} \int \left[\int y dF_{Y|X,T}(y, x, t) - a_1^T(x - \mu_X(t)) - \beta_0 - \beta_1(s - t) \right]^2 \times \\ & \qquad \qquad \qquad K_h(s - t) dF_{X,T}(x, s). \end{aligned}$$

Defining as before the following auxiliary parameters for $j = 0, 1, 2$,

$$\begin{aligned} \mu_{0j} &:= E(K_h(T - t)(T - t)^j), \\ \Sigma_{2j} &:= E(K_h(T - t)(T - t)^j(X(T) - \mu_X(t))(X(T) - \mu_X(t))^T), \\ r_{0j} &:= E(K_h(T - t)(T - t)^j Y), \\ r_{1j} &:= E(K_h(T - t)(T - t)^j Y(X(T) - \mu_X(t))), \\ \sigma_0^2 &:= \mu_{02}\mu_{00} - \mu_{01}^2. \end{aligned}$$

and solving the minimization problem leads to

$$a_1^* = \Sigma_{20}^{-1} r_{10}, \quad \beta_0^* = \frac{r_{00}\mu_{02} - r_{01}\mu_{01}}{\sigma_0^2}, \quad \beta_1^* = \frac{r_{01}\mu_{00} - r_{00}\mu_{01}}{\sigma_0^2}.$$

Putting the optimal values of the parameters back in the model,

$$\begin{aligned} \tilde{g}(x, t) &= a_1^*(x, t)(x - \mu_X(t)) + \beta_0^*(x, t) = \int s^G(z, x, s, t, h) y dF(y, z, s) \\ & E(s^G(X, x, T, t, h) Y) \end{aligned}$$

with weight function,

$$s^G(z, x, s, t, h) = \underbrace{K_h(s-t) [(z - \mu_X(t))^T \Sigma_{20}^{-1} (x - \mu_X(t))]}_{:=s_1(z, x, s, t, h)} + \underbrace{\frac{1}{\sigma_0^2} K_h(s-t) (\mu_{02} - (s-t)\mu_{01})}_{:=s_2(s, t, h)}$$

Rewriting the framework as the weighted Fréchet mean w.r.t the Euclidean metric,

$$\begin{aligned} \tilde{g}(x, t) &= \operatorname{argmin}_{y \in \mathbb{R}} E (s^G(X, x, T, t, h)(Y - y)^2) \\ &= \operatorname{argmin}_{y \in \mathbb{R}} E (s^G(X, x, T, t, h)d_E^2(Y, y)), \end{aligned}$$

where \tilde{g} can be viewed as a smoothed version of the true regression function m with bias $m(x, t) - \tilde{g}(x, t) = o(1)$. This alternative formulation of the combination of a global and a local regression component thus provides the intuition to define the general population model for metric-space valued random objects as

$$\tilde{g}_\oplus(x, t) = \operatorname{argmin}_{\omega \in \Omega} \tilde{G}_\oplus(\omega), \text{ where, } \tilde{G}_\oplus(\omega) := E (s^G(X, x, T, t, h)d^2(Y, \omega)). \quad \square$$

D.3. Technical assumptions (B1)-(B6) and (U1)-(U4) in section 4

The following is a list of these assumptions which are required for section 4.

- (B1) The kernel function K is a univariate probability density that is symmetric around zero, with $|K_{0j}^\gamma| = |\int K^\gamma(u)u^j du| < \infty$ for $j = 1, \dots, 4$ and $\gamma = 0, 1, 2$.
- (B2) The marginal density $f_{(X,T)}(x, t)$ and the conditional density $f_{(X,T)|Y}(x, t, y)$ exist, are twice continuously differentiable as a function of t for all x and all y .
- (B3) The Fréchet means $m_\oplus(x, t), \tilde{g}_\oplus(x, t), \hat{g}_\oplus(x, t)$ exist and are unique.
- (B4) For any $\epsilon > 0$,

$$\inf_{d(\omega, m_\oplus(x, t)) > \epsilon} (M_\oplus(\omega, x, t) - M_\oplus(m_\oplus(x, t), x, t)) > 0.$$

$$\inf_{d(\omega, \tilde{g}_\oplus(x, t)) > \epsilon} (\tilde{G}_\oplus(\omega, x, t) - \tilde{G}_\oplus(\tilde{g}_\oplus(x, t), x, t)) > 0.$$

- (B5) There exist $\eta_1 > 0, C_1 > 0$, with $d(\omega, m_\oplus(x, t)) < \eta_1$ such that

$$M_\oplus(\omega, x, t) - M_\oplus(m_\oplus(x, t), x, t) \geq C_1 d(\omega, m_\oplus(x, t))^2.$$

- (B6) There exist $\eta_2 > 0, C_2 > 0$, with $d(\omega, \tilde{g}_\oplus(x, t)) < \eta_2$ such that

$$\liminf_N \left[\tilde{G}_\oplus(\omega, x, t) - \tilde{G}_\oplus(\tilde{g}_\oplus(x, t), x, t) \right] \geq C_1 d(\omega, \tilde{g}_\oplus(x, t))^2.$$

These assumptions are required to ensure the existence and uniqueness of the Fréchet mean in the population and sample cases and the local curvature of the objective functions near their respective minimums to establish consistency of the partially global concurrent object regression (CORE) estimator. Also the relevant entropy conditions are necessary to prove the rate of convergence of the CORE estimator.

For proving the uniform convergence results in the X -direction for any fixed value of t , the following additional conditions are used.

- (U1) For almost all x such that $\|x\|_E \leq M$, the Fréchet means $m_{\oplus}(x, t)$, $\tilde{g}_{\oplus}(x, t)$, $\hat{g}_{\oplus}(x, t)$ exist and are unique.
- (U2) For any $\epsilon > 0$,

$$\inf_{\|x\|_E \leq Md(\omega, m_{\oplus}(x, t)) > \epsilon} \inf (M_{\oplus}(\omega, x, t) - M_{\oplus}(m_{\oplus}(x, t), x, t)) > 0.$$

Also, there exists $\zeta = \zeta(\epsilon)$ such that

$$P \left(\inf_{\|x\|_E \leq Md(\omega, \hat{g}_{\oplus}(x, t)) > \epsilon} \hat{G}_{\oplus}(\omega, x, t) - \hat{G}_{\oplus}(\hat{g}_{\oplus}(x, t), x, t) \geq \zeta \right) \rightarrow 1.$$

- (U3) With $\mathcal{B}_{\delta}(m_{\oplus}(x, t))$ and $N(\epsilon, \mathcal{B}_{\delta}(m_{\oplus}(x, t)), d)$, as defined in Assumption (A7)

$$\int_0^1 \sup_{\|x\|_E \leq M} \sqrt{1 + \log N(\delta\epsilon, \mathcal{B}_{\delta}(m_{\oplus}(x, t)), d)} d\epsilon = O(1) \text{ as } \delta \rightarrow 0.$$

- (U4) There exist constants $\tau > 0, D > 0$ and $\alpha > 2$ possibly depending on M such that, for any given t ,

$$\inf_{\|x\|_E \leq Md(\omega, m_{\oplus}(x, t)) < \tau} [M_{\oplus}(\omega, x, t) - M_{\oplus}(m_{\oplus}(x, t), x, t) - Dd(\omega, m_{\oplus}(x, t))] \geq 0.$$

D.4. Proofs for section 4

We use $\mu_{0j} = E(K_h(T - t)(T - t)^j)$ and $\tau_{0j} := E(K_h(T - t)(T - t)^j | Y = y)$.

Lemma D.5. Under assumptions (B1)- (B2),

$$\begin{aligned} \mu_{0j} &= h^j \left[f_{X,T}(x, t)K_{0j} + hK_{0(j+1)} \left(\frac{\partial}{\partial t} f_{X,T}(x, t) \right) \Big|_{t=t} + O(h^2) \right], \\ \tau_{0j} &= h^j \left[f_{X,T|Y}(x, t, y)K_{0j} + hK_{0(j+1)} \left(\frac{\partial}{\partial t} f_{X,T|Y}(x, t, y) \right) \Big|_{t=t} + O(h^2) \right]. \end{aligned}$$

This holds for all x , and in the case of τ_{0j} , the error term is uniform over all $y \in \Omega$.

Proof. This follows from a second-order Taylor expansion in the second argument at $t = t$, under the assumption that the densities exist and are twice continuously differentiable in the T - direction for all $X = x$. \square

Proof of Proposition 4.1. Observe that

- (i) Since $\mu_X(t) = E_{X|T=t}(X) = E(X(t)|T = t)$ recalling the fact that $\int s_1(z, x, s, t, h) dF_{X,T}(z, s) = 0$, we have,

$$\begin{aligned} & \int d^2(y, \omega) s_1(z, x, s, t, h) dF_{X,T,Y}(z, s, y) \\ &= \int d^2(y, \omega) \left(\int s_1(z, x, s, t, h) dF_{(X,T)|Y}(z, s, y) \right) dF_Y(y) = 0. \end{aligned}$$

- (ii) By a similar argument as Lemma D.2 and using Lemma D.5 we find

$$\begin{aligned} & \int s_2(s, t, h) dF_{X,T|Y}(x, s, y) \\ &= \int \frac{1}{\sigma_0^2} K_h(s - t) (\mu_{02} - (s - t)\mu_{01}) dF_{X,T|Y}(x, s, y) \\ &= \frac{\tau_{00}(y) \mu_{02} - \tau_{01}(y) \mu_{01}}{\sigma_0^2} = \frac{f_{X,T|Y}(x, s, y)}{f_{X,T}(x, s)} + O(h^2) \\ &= \frac{dF_{Y|(X,T)}(y, x, s)}{dF_Y(y)} + O(h^2). \end{aligned}$$

Hence, proceeding similarly as in Proposition 3.2,

$$\begin{aligned} & \int d^2(y, w) s^G(z, x, s, t, h) dF_{X,T,Y}(x, s, y) \\ &= \int d^2(y, w) s_1(z, x, s, t, h) dF_{X,T,Y}(x, s, y) \\ & \quad + \int d^2(y, w) s_2(s, t, h) dF_{X,T,Y}(x, s, y) \\ &= \int d^2(y, w) \left(\frac{dF_{Y|(X,T)}(y, x, s)}{dF_Y(y)} + O(h^2) \right) dF_Y(y) \\ &= M_{\oplus}(\omega, x, t) + O(h^2). \end{aligned}$$

Thus, minimizing \tilde{G}_{\oplus} is approximately the same as minimizing the conditional Fréchet function M_{\oplus} . Since the error term is uniform over $y \in \Omega$ by assumptions (B3)-(B4) concerning the existence and uniqueness of the minimizer of the respective objective functions, we have $d(m_{\oplus}(x, t) - \tilde{g}_{\oplus}(x, t)) = o(1)$ as $h = h_n \rightarrow 0$. The rate of convergence, hence the result follows using a similar technique as in the proof of Proposition 3.1. \square

Proof of Proposition 4.2. Using the empirical weight function defined in (4.3)-(4.6),

$$\hat{s}_{il}^G = \underbrace{K_h(T_{il} - t)(X_{il} - \hat{\mu}_X(t))^T \hat{\Sigma}_{20}^{-1}(x - \hat{\mu}_X(t))}_{:= \hat{s}_{(1)il}}$$

$$+ \underbrace{\frac{1}{\hat{\sigma}_0^2} [K_h(T_{il} - t)\hat{\mu}_{20} - (T_{il} - t)\hat{\mu}_{10}]}_{:=\hat{s}_{(2)il}}, \tag{D.12}$$

and a set of auxiliary weight parameters

$$s_{il}^G = \underbrace{K_h(T_{il} - t)(X_{il} - \mu_X(t))^T \Sigma_{20}^{-1}(x - \mu_X(t))}_{:=s_{(1)il}} + \underbrace{\frac{1}{\sigma_0^2} K_h(T_{il} - t) [\mu_{20} - (T_{il} - t)\mu_{10}]}_{:=s_{(2)il}}. \tag{D.13}$$

Note that the weight functions above is a sum of into two separate weight functions. We observe that,

$$\hat{s}_{il}^G - s_{il}^G = (U_0 K_h(T_{il} - t) + U_1^T X_{il} K_h(T_{il} - t)) + (V_0 K_h(T_{il} - t) + V_1 K_h(T_{il} - t)(T_{il} - t)),$$

where

$$\begin{aligned} U_0 &= U_0(x, t) := (\hat{\mu}_X(t))^T \Sigma_{20}^{-1}(x - \hat{\mu}_X(t)) - (\mu_X(t))^T \Sigma_{20}^{-1}(x - \mu_X(t)); \\ U_1 &= U_1(x, t, h) := \Sigma_{20}^{-1}(x - \mu_X(t)) - \hat{\Sigma}_{20}^{-1}(x - \hat{\mu}_X(t)); \\ V_0 &= V_0(t, h) := \frac{\hat{\mu}_{02}}{\hat{\sigma}_0^2} - \frac{\mu_{02}}{\sigma_0^2}; \\ V_1 &= V_1(t, h) := \frac{\hat{\mu}_{10}}{\hat{\sigma}_0^2} - \frac{\mu_{10}}{\sigma_0^2}. \end{aligned}$$

Then the difference $\hat{G}_\oplus(\omega) - \tilde{G}_\oplus(\omega)$ can be written as

$$\begin{aligned} \hat{G}_\oplus(\omega) - \tilde{G}_\oplus(\omega) &= \frac{1}{n} \sum_{i=1}^n \left(\frac{1}{n_i} \sum_{l=1}^{n_i} [\hat{s}_{il}^G(x, t, h) - s_{il}^G(x, t, h)] d^2(Y_{il}, \omega) \right) \\ &+ \frac{1}{n} \sum_{i=1}^n \left(\frac{1}{n_i} \sum_{l=1}^{n_i} [s_{il}^G(x, t, h) d^2(Y_{il}, \omega) - E(s_{il}^G(x, t, h) d^2(Y_{il}, \omega))] \right). \end{aligned} \tag{D.14}$$

For $\hat{\mu}_X(t)$ being a local linear estimator of $\mu_X(\cdot)$ at any given point t we have $\hat{\mu}_X(t) = O_P((nh)^{-1/2})$ [66]. This implies that $U_0 = O_P((nh)^{-1/2})$ and $\hat{\Sigma}_{20} = O_P((nh)^{-1/2})$. Hence $\|U_1\|_E = O_P((nh)^{-1/2})$. Also, using Lemma D.5 we have, $V_0 = O_P((nh)^{-1/2})$, $V_1 = O_P((nh^3)^{-1/2})$. Since

$$\begin{aligned} E(K_h(T_{il} - t)(T_{il} - t)^j d^2(Y_{il}, \omega) X_{il}) &= O(h^j), \\ E(K_h^2(T_{il} - t)(T_{il} - t)^{2j} d^4(Y_{il}, \omega) X_{il}) &= O(h^{2j-1}), \end{aligned}$$

the first term in the above equation is $O_P((nh)^{-1/2})$ and also, $E((s_{il}^G(x, t, h))^2) = O(h^{-1})$ which implies that the second term in equation (D.14) is also

$O_P((nh)^{-1/2})$. Thus we have $\hat{G}_\oplus(\omega) - \tilde{G}_\oplus(\omega) = o_P(1)$ for any $\omega \in \Omega$ as $nh \rightarrow \infty$. Following the same arguments as in the proof of Proposition 3.2 the claim follows and then Theorem 4.1, using Propositions 4.1 and 4.2. \square

Proof of Theorem 4.2. For any given local point t in the T -direction, consider the process, $\{Z_n(x) := d(\hat{g}_\oplus(x, t), \tilde{g}_\oplus(x, t)); x \in \mathbb{R}^p : \|x\|_E \leq M \text{ for some } M > 0\}$. From Theorem 4.1, $Z_n(x) = o_P(1)$. To show the uniform convergence of $\{Z_n(x)\}$ using Theorem 1.5.4 of [58] we need to show the asymptotic equicontinuity of $\{Z_n(x)\}$, that is, for any $S > 0$ and $\delta \rightarrow 0$,

$$\limsup_{n \rightarrow \infty} P \left(\sup_{\substack{\|x-y\|_E < \delta \\ \|x\|_E \leq M, \|y\|_E \leq M}} |Z_n(x) - Z_n(y)| > 2S \right) \rightarrow 0.$$

Since, for any given $t \in \mathcal{T}$,

$|Z_n(x) - Z_n(y)| \leq d(\hat{g}_\oplus(x, t), \hat{g}_\oplus(y, t)) + d(\tilde{g}_\oplus(x, t), \tilde{g}_\oplus(y, t))$, it suffices to show that $\tilde{g}_\oplus(x, t)$ is uniformly continuous for $\|x\|_E \leq M$ and for any $S > 0$ and $\delta \rightarrow 0$,

$$\limsup_{n \rightarrow \infty} P \left(\sup_{\substack{\|x-y\|_E < \delta \\ \|x\|_E \leq M, \|y\|_E \leq M}} d(\hat{g}_\oplus(x, t), \hat{g}_\oplus(y, t)) > 2S \right) \rightarrow 0.$$

We observe that, for $\delta > 0$ and $x, y \in \mathbb{R}^p$ with $\|x - y\|_E < \delta$,

$$\begin{aligned} & \sup_{\omega \in \Omega} |\tilde{G}_\oplus(\omega, x, t) - \tilde{G}_\oplus(\omega, y, t)| \\ &= \sup_{\omega \in \Omega} |E((s^G(X, x, T, t, h) - s^G(X, y, T, t, h))d^2(Y, w))| \\ &= \sup_{\omega \in \Omega} |E((X - \mu_X(t))^T \Sigma_{20}^{-1}(x - y)d^2(Y, w))| \rightarrow 0 \text{ as } \delta \rightarrow 0. \end{aligned}$$

This, combined with Assumption (U2) implies that, for any given t , $\tilde{g}_\oplus(x, t)$ is continuous at every x in the compact set where $\|x\|_E \leq M$, hence is uniformly continuous over $\{x \in \mathbb{R}^p : \|x\|_E \leq M\}$. Finally, to show the asymptotic equicontinuity of $d(\hat{g}_\oplus(x, t), \hat{g}_\oplus(y, t))$, let us assume, for any $\epsilon > 0$ and $\|x\|_E, \|y\|_E \leq M$, $d(\hat{g}_\oplus(x, t), \hat{g}_\oplus(y, t)) > \epsilon$. Then using the form of the corresponding objective function, $\hat{G}(\omega, x, t)$, we have,

$$\sup_{\substack{\|x-y\|_E < \delta \\ \|x\|_E \leq M, \|y\|_E \leq M}} \sup_{\omega \in \Omega} |\hat{G}(\omega, x, t) - \hat{G}(\omega, y, t)| = O_P(\delta).$$

However, this is a contradiction to Assumption (U2) as $\delta \rightarrow 0$ and thus first result follows. Let us write $V_n(\omega) = \hat{G}_\oplus(\omega, x, t) - G_\oplus(\omega, x, t)$. Thus defining $D_{il} = d^2(Y_{il}, \omega) - d^2(Y_{il}, \tilde{g}_\oplus(x, t))$, for any given $t \in \mathcal{T}$, we have

$$|V_n(\omega) - V_n(\tilde{g}_\oplus(x, t))| \leq \left| \frac{1}{n} \sum_{i=1}^n \frac{1}{n_i} \sum_{l=1}^{n_i} [\hat{s}_{il}^G(x, t, h) - s_{il}^G(x, t, h)] D_{il}(\omega, x, t) \right|$$

$$+ \left| \frac{1}{n} \sum_{i=1}^n \frac{1}{n_i} \sum_{l=1}^{n_i} [s_{il}^G(x, t, h)D_{il} - E(s_{il}^G D_{il})] \right| \quad (\text{D.15})$$

Note that $U_0(x, t)$ and $U_1(x, t)$, as described in the proof of Proposition 4.1, are respectively $O_P(n^{-1/2})$ and $O_P((nh)^{-1/2})$, uniformly over $\|x\|_E \leq M$. Then

$$\begin{aligned} & \sup_{\|x\|_E \leq M} \sup_{d(\omega, g_{\oplus}(x, t)) < \delta} \left| \frac{1}{n} \sum_{i=1}^n \frac{1}{n_i} \sum_{l=1}^{n_i} [\hat{s}_{il}^G(x, t) - s_{il}^G(x, t)] D_{il}(\omega, x, t) \right| \\ &= O_P\left(\delta(nh)^{-1/2}\right). \end{aligned} \quad (\text{D.16})$$

We can define,

$$\begin{aligned} A_R = & \left\{ \sup_{\|x\|_E \leq M} \sup_{d(\omega, g_{\oplus}(x, t)) < \delta} \left| \frac{1}{n} \sum_{i=1}^n \frac{1}{n_i} \sum_{l=1}^{n_i} [\hat{s}_{il}^G(x, t) - s_{il}^G(x, t)] D_{il}(\omega, x, t) \right| \right. \\ & \left. \leq R\delta(nh)^{-1/2} \right\}, \end{aligned}$$

for $R > 0$, so that $P(A_R^c) \rightarrow 0$. As for the second term on the right hand side of (D.15),

$$\begin{aligned} & \left| \frac{1}{n} \sum_{i=1}^n \frac{1}{n_i} \sum_{l=1}^{n_i} [s_{il}^G(x, t, h)D_{il} - E(s_{il}^G D_{il})] \right| \\ & \leq \left| \frac{1}{n} \sum_{i=1}^n \frac{1}{n_i} \sum_{l=1}^{n_i} [s_{(1)il}(x, t, h)D_{il} - E(s_{(1)il} D_{il})] \right| \\ & \quad + \left| \frac{1}{n} \sum_{i=1}^n \frac{1}{n_i} \sum_{l=1}^{n_i} [s_{(2)il}(x, t, h)D_{il} - E(s_{(2)il} D_{il})] \right|, \end{aligned} \quad (\text{D.17})$$

where $s_{il}^G = s_{(1)il} + s_{(2)il}$ as described in (D.13). Similar to (D.10) in the proof of Proposition 3.2 one can show that the second term in the right hand side of (D.17) is bounded, i.e.,

$$\left| \frac{1}{n} \sum_{i=1}^n \frac{1}{n_i} \sum_{l=1}^{n_i} [s_{(2)il}(x, t, h)D_{il} - E(s_{(2)il} D_{il})] \right| = O\left(\delta(nh)^{-1/2}\right). \quad (\text{D.18})$$

Also, we can bound the first term on the right hand side of (D.16) by

$$\begin{aligned} & \left| \frac{1}{n} \sum_{i=1}^n \frac{1}{n_i} \sum_{l=1}^{n_i} [s_{(1)il}(x, t, h)D_{il} - E(s_{(1)il} D_{il})] \right| \\ & \leq \|\Sigma_{20}^{-1}(t)(x - \mu_X(t))\|_E \times \\ & \quad \sum_{j=1}^p \left| \frac{1}{n} \sum_{l=1}^{n_i} n_i^{-1} (X_{il}^{(j)} - \mu_X(t)^{(j)}) D_{il}(\omega, x, t) - E((X_{il}^{(j)} - \mu_X(t)^{(j)}) D_{il}(\omega, x, t)) \right| \end{aligned}$$

$$+ \left| \frac{1}{n} \sum_{l=1}^{n_i} n_i^{-1} D_{il}(\omega, x, t) - E(D_{il}(\omega, x, t)) \right|,$$

where $(X_{il}^{(j)})$ $\mu_X(t)^{(j)}$ denote the j^{th} component of X_{il} and $\mu_X(t)$ respectively. Following a similar line of argument for finding a class of envelope functions to control the covering number required in the entropy integral in Assumption (U3) one can show that,

$$E \left(\sup_{\|x\| \leq M} \sup_{d(\omega, \tilde{g}_{\oplus}(x, t)) < \delta} \left| \frac{1}{n} \sum_{i=1}^n \frac{1}{n_i} \sum_{l=1}^{n_i} [s_{(1)il}(x, t, h) D_{il} - E(s_{(1)il} D_{il})] \right| \right) = O \left(\delta^\gamma (nh)^{-1/2} \right), \quad (\text{D.19})$$

for any $\gamma < 1$. Thus combining (D.16), (D.18), and (D.19) in (D.15) we have, for each given $t \in \mathcal{T}$,

$$E \left(\mathbf{1}(A_R) \sup_{\|x\| \leq M} \sup_{d(\omega, \tilde{g}_{\oplus}(x, t)) < \delta} \|V_n(\omega) - V_n(\tilde{g}_{\oplus}(x, t))\| \right) \leq b \delta^\gamma (nh)^{-1/2},$$

for some constant $b = b(\gamma)$. For $\alpha > 2$ as defined in Assumption (U4) such that for any $\alpha' > \alpha$ and $\gamma = 1 + \alpha - \alpha'$, following the point-wise rate argument, one can show that

$$\sup_{\|x\| \leq M} d(\hat{g}_{\oplus}(x, t), \tilde{g}_{\oplus}(x, t)) = O_P \left((nh)^{-\frac{1}{2(\alpha' - 1)}} \right) = .O_P \left((nh)^{-1/2 + \delta} \right),$$

for any $\delta > 0$. Finally, the bias term introduced by changing the target from m_{\oplus} in (2.1) to g_{\oplus} in (4.1) can be shown as $O(h^2)$ uniformly over $\|x\|_E \leq M$ for each given $t \in T$, using the uniform equi-continuity of \tilde{g}_{\oplus} and the total boundedness of the space Ω . Combining these the result follows. \square

Appendix E: Additional figures

We present here some additional figures that are referred to in the main paper in the context of simulation studies and real data applications in Sections 5 and 6 respectively.

Additional figure from simulation studies in Section 5

The performance of the proposed partially global concurrent object regression (CORE) model is compared to the global Fréchet regression (GFR) method from [44]. In the latter, the nested structure of the predictor space $(T, X(T))$ is ignored and thus $T \in \mathbb{R}$ and $X \in \mathbb{R}^p$ are treated as a $p + 1$ dimensional predictor input for the model. The data generating mechanism is as described in Setting I of Section 5.1, with the each component of the predictor process $X(\cdot) \in \mathbb{R}^p$ assumed to be uncorrelated. The proposed partially global CORE method outperforms GFR in all cases.

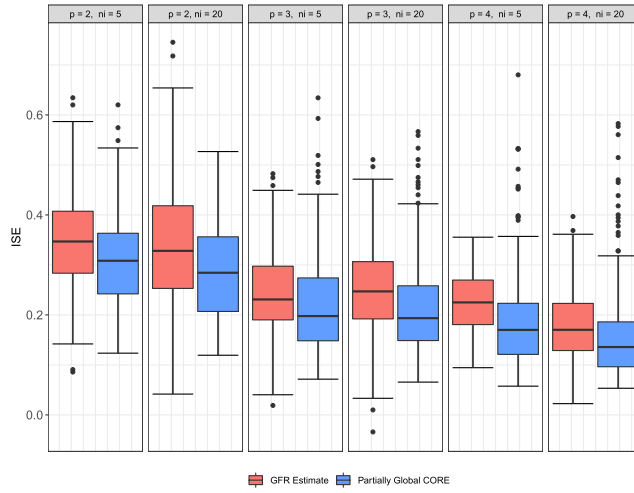


FIG 16. Figure shows the comparative performance of the proposed partially global concurrent object regression (CORE) method to that of global Fréchet regression (GFR) with increasing the predictor dimension p for distributional object responses. The sample sizes are kept fixed at $n = 1000$ and dense and sparse designs are considered with $n_i = 5$ and $n_i = 20$ respectively.

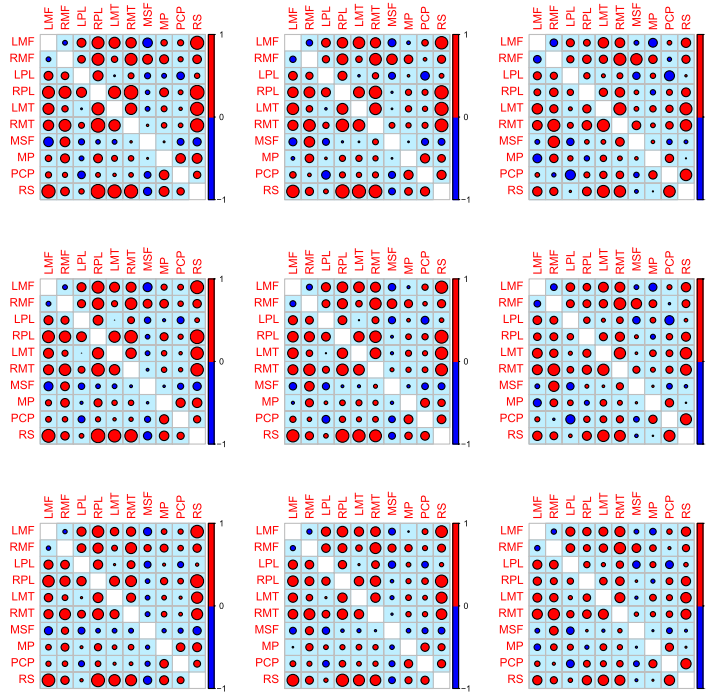


FIG 17. Estimated correlation matrix for the CN subjects fitted locally using nonparametric CORE in (3.8) illustrating the dependence of functional connectivity on total cognitive score which gets modulated by age. The arrangement of the panels are the same as that of Figure 4.

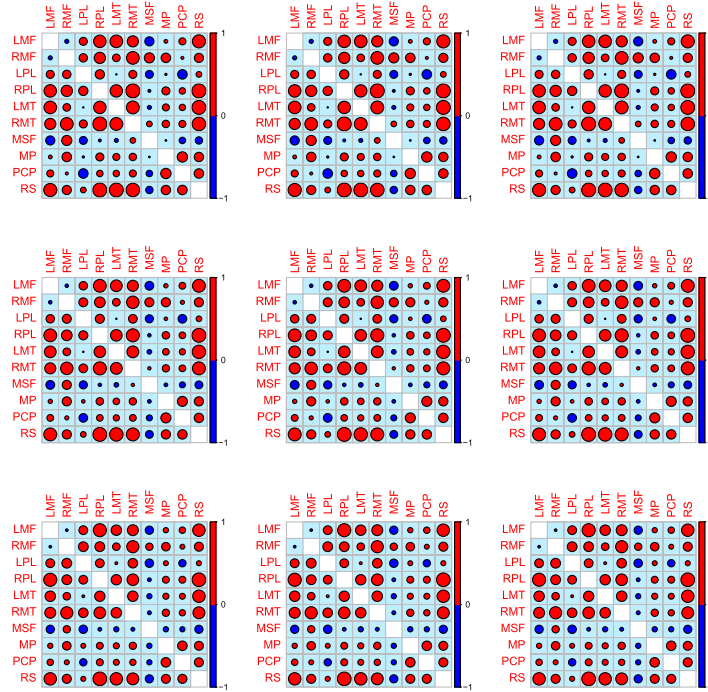


FIG 18. *Estimated correlation matrix for the CN subjects fitted locally using partially global CORE in (4.1) illustrating the dependence of functional connectivity on total cognitive score which gets modulated by age. The arrangement of the panels are the same as that of Figure 4.*

Additional figures from real-data applications in Section 6

The following figures show additional illustrations for the data application for brain connectivity in Alzheimer's disease in Section 6.1, where pairwise connectivity correlation matrices are considered as random object responses varying with age, and the predictors taken were age and total cognitive score changing with age.

Figure 17 displays the connectivity correlation matrices for the CN subjects, estimated using the nonparametric CORE method locally over a range of different output points. This elicits a the regression relationship between the functional connectivity matrix and the total cognitive scores in Section 6.1, which is further altered by age. Quite contrary to the case of the AD subjects (4), here we observe a prominence of positive correlations between the brain parcellation throughout, in terms of stronger magnitude and higher number. This might well be indicative of a better inter-hub functional connectivity in the CN subjects. Over increasing age we observe a higher value for the total cognitive score which can be associated with a weaker inter-hub connectivity overall. The reduction in Negative Functional Correlation (NFC) for CN subjects is still noted but the evolution is not so drastic over age. In addition, the estimated correlation

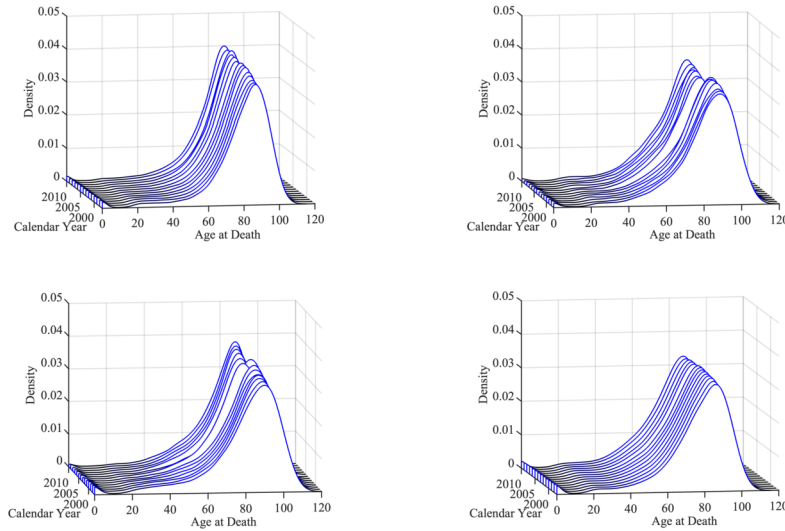


FIG 19. The observed time-varying age at death density functions over the years for males in Australia, Finland, U.S. and Portugal, clockwise in the four panels, starting at the upper left.

matrices for the CN subjects exhibit specific patterns of dependency over the connectivity hubs, which, in case of the estimated correlation matrices for the AD subjects is not as discernible. A further application of the partially global model gives evidence along the same line as the nonparametric CORE model (Figure 18). However, the in-sample goodness of fit measured by the integrated deviance statistic (see (6.2) in Section 6.1) for the former (0.0056) is marginally better than the latter (0.0071), accounting for a better performance of the partially global Model.

The following figure is an additional illustration for the real data application for impact of GDP on human mortality, where a sample of age-at-death densities were treated as the distributional object responses varying with calendar years for 22 countries and GDP data of each country, for changing calendar year were considered as predictors. The figure shows the 3D plots for the observed age-at-death distributions, represented as densities, over the years for four countries—Australia, Finland, Portugal and the U.S., as is referred to in the main paper in Section 6.2.

Acknowledgments

Data collection and sharing for this project was funded by the Alzheimer’s Disease Neuroimaging Initiative (ADNI) (National Institutes of Health Grant U01 AG024904) and DOD ADNI (Department of Defense award number W81XWH-12-2-0012). As such, the investigators within the ADNI contributed to the design and implementation of ADNI and/or provided data but did not participate

in analysis or writing of this report. A complete listing of ADNI investigators can be found at: http://adni.loni.usc.edu/wp-content/uploads/how_to_apply/ADNIAcknowledgement_List.pdf.

The authors would like to thank the reviewers for helpful comments that led to numerous improvements.

References

- [1] AFSARI, B. (2011). Riemannian L^p center of mass: existence, uniqueness, and convexity. *Proceedings of the American Mathematical Society* **139** 655–673. [MR2736346](#)
- [2] ALLEN, E., DAMARAJU, E., PLIS, S., ERHARDT, E., EICHELE, T. and CALHOUN, V. (2014). Tracking whole-brain connectivity dynamics in the resting state. *Cerebral Cortex* **24** 663–676.
- [3] ARSIGNY, V., FILLARD, P., PENNEC, X. and AYACHE, N. (2007). Geometric means in a novel vector space structure on symmetric positive-definite matrices. *SIAM Journal on Matrix Analysis and Applications* **29** 328–347. [MR2288028](#)
- [4] BHATTACHARYA, R. and PATRANGENARU, V. (2003). Large sample theory of intrinsic and extrinsic sample means on manifolds. *Annals of Statistics* **31**. [MR1962498](#)
- [5] BHATTACHARYA, R. and PATRANGENARU, V. (2005). Large sample theory of intrinsic and extrinsic sample means on manifolds: II. *Annals of Statistics*. [MR2195634](#)
- [6] BICKEL, P. J., LI, B. et al. (2007). Local polynomial regression on unknown manifolds. In *Complex Datasets And Inverse Problems* 177–186. Institute of Mathematical Statistics. [MR2459188](#)
- [7] BILLERA, L. J., HOLMES, S. P. and VOGTMANN, K. (2001). Geometry of the space of phylogenetic trees. *Advances in Applied Mathematics* **27** 733–767. [MR1867931](#)
- [8] BRIER, M. R., THOMAS, J. B., SNYDER, A. Z., BENZINGER, T. L., ZHANG, D., RAICHEL, M. E., HOLTZMAN, D. M., MORRIS, J. C. and ANCES, B. M. (2012). Loss of intranetwork and internetwork resting state functional connections with Alzheimer’s disease progression. *Journal of Neuroscience* **32** 8890–8899.
- [9] BUCKNER, R. L., SEPULCRE, J., TALUKDAR, T., KRIENEN, F. M., LIU, H., HEDDEN, T., ANDREWS-HANNA, J. R., SPERLING, R. A. and JOHNSON, K. A. (2009). Cortical hubs revealed by intrinsic functional connectivity: mapping, assessment of stability, and relation to Alzheimer’s disease. *Journal of Neuroscience* **29** 1860–1873.
- [10] CHEN, Y., LIN, Z. and MÜLLER, H.-G. (2021). Wasserstein regression. *Journal of the American Statistical Association* 1–14.
- [11] CHIANG, C.-T., RICE, J. A. and WU, C. O. (2001). Smoothing spline estimation for varying coefficient models with repeatedly measured dependent variables. *Journal of the American Statistical Association* **96** 605–619. [MR1946428](#)

- [12] CLEVELAND, W. S., GROSSE, E. and SHYU, W. M. (2017). Local regression models. In *Statistical Models In S* 309–376. Routledge.
- [13] CORNEA, E., ZHU, H., KIM, P. and IBRAHIM, J. G. (2017). Regression models on Riemannian symmetric spaces. *Journal of the Royal Statistical Society Series B* **79** 463–482. [MR3611755](#)
- [14] DAMOISEAUX, J. S., PRATER, K. E., MILLER, B. L. and GREICIUS, M. D. (2012). Functional connectivity tracks clinical deterioration in Alzheimer’s disease. *Neurobiology of Aging* **33** 828–e19.
- [15] DAVIS, B. C., FOSKEY, M., ROSENMAN, J., GOYAL, L., CHANG, S. and JOSHI, S. (2005). Automatic segmentation of intra-treatment CT images for adaptive radiation therapy of the prostate. In *International Conference on Medical Image Computing and Computer-Assisted Intervention* 442–450. Springer.
- [16] DI MARZIO, M., PANZERA, A. and TAYLOR, C. C. (2014). Nonparametric regression for spherical data. *Journal of the American Statistical Association* **109** 748–763. [MR3223747](#)
- [17] DRYDEN, I. L., PENNEC, X. and PEYRAT, J.-M. (2010). Power Euclidean metrics for covariance matrices with application to diffusion tensor imaging. *arXiv preprint arXiv:1009.3045*.
- [18] DRYDEN, I. L., KOLOYDENKO, A., ZHOU, D. et al. (2009). Non-Euclidean statistics for covariance matrices, with applications to diffusion tensor imaging. *Annals of Applied Statistics* **3** 1102–1123. [MR2750388](#)
- [19] DRYDEN, I. L., KOLYDENKO, A., ZHOU, D. and LI, B. (2010). Non-Euclidean statistical analysis of covariance matrices and diffusion tensors. *arXiv preprint arXiv:1010.3955*. [MR2750388](#)
- [20] EUBANK, R., HUANG, C., MALDONADO, Y. M., WANG, N., WANG, S. and BUCHANAN, R. (2004). Smoothing spline estimation in varying-coefficient models. *Journal of the Royal Statistical Society: Series B (Statistical Methodology)* **66** 653–667. [MR2088294](#)
- [21] FAN, J. and GIJBELS, I. (1996). *Local Polynomial Modelling and its Applications: Monographs on Statistics and Applied Probability 66*. Routledge. [MR1383587](#)
- [22] FAN, J. and ZHANG, W. (1999). Statistical estimation in varying coefficient models. *Annals of Statistics* **27** 1491–1518. [MR1742497](#)
- [23] FAN, J. and ZHANG, J.-T. (2000). Two-step estimation of functional linear models with applications to longitudinal data. *Journal of the Royal Statistical Society: Series B (Statistical Methodology)* **62** 303–322. [MR1749541](#)
- [24] FAN, J. and ZHANG, W. (2008). Statistical methods with varying coefficient models. *Statistics and its Interface* **1** 179. [MR2425354](#)
- [25] FERREIRA, L. R. K. and BUSATTO, G. F. (2013). Resting-state functional connectivity in normal brain aging. *Neuroscience & Biobehavioral Reviews* **37** 384–400.
- [26] FRÉCHET, M. R. (1948). Les éléments aléatoires de nature quelconque dans un espace distancié. *Annales de l’institut Henri Poincaré* **10** 215–310. [MR0027464](#)
- [27] HASTIE, T. and TIBSHIRANI, R. (1993). Varying-coefficient models. *Jour-*

- nal of the Royal Statistical Society. Series B (Methodological)* **55** 757–796. [MR1229881](#)
- [28] HOOVER, D. R., RICE, J. A., WU, C. O. and YANG, L.-P. (1998). Non-parametric smoothing estimates of time-varying coefficient models with longitudinal data. *Biometrika* **85** 809–822. [MR1666699](#)
- [29] HORVÁTH, L. and KOKOSZKA, P. (2012). *Inference For Functional Data With Applications*. Springer Science & Business Media. [MR2920735](#)
- [30] HUANG, J. Z., WU, C. O. and ZHOU, L. (2002). Varying-coefficient models and basis function approximations for the analysis of repeated measurements. *Biometrika* **89** 111–128. [MR1888349](#)
- [31] KLOECKNER, B. (2010). A geometric study of Wasserstein spaces: Euclidean spaces. *Annali della Scuola Normale Superiore di Pisa-Classe di Scienze* **9** 297–323. [MR2731158](#)
- [32] KUEPER, J. K., SPEECHLEY, M. and MONTERO-ODASSO, M. (2018). The Alzheimer’s disease assessment scale–cognitive subscale (ADAS-Cog): modifications and responsiveness in pre-dementia populations. a narrative review. *Journal of Alzheimer’s Disease* **63** 423–444.
- [33] LIN, Z. (2019). Riemannian geometry of symmetric positive definite matrices via Cholesky decomposition. *SIAM Journal on Matrix Analysis and Applications* **40** 1353–1370. [MR4032859](#)
- [34] MAITY, A. (2017). Nonparametric functional concurrent regression models. *Wiley Interdisciplinary Reviews: Computational Statistics* **9** e1394. [MR3615675](#)
- [35] MANRIQUE, T., CRAMBES, C. and HILGERT, N. (2018). Ridge regression for the functional concurrent model. *Electronic Journal of Statistics* **12** 985–1018. [MR3776278](#)
- [36] MARRON, J. S. and ALONSO, A. M. (2014). Overview of object oriented data analysis. *Biometrical Journal* **56** 732–753. [MR3258083](#)
- [37] MOAKHER, M. (2005). A differential geometric approach to the geometric mean of symmetric positive-definite matrices. *SIAM Journal on Matrix Analysis and Applications* **26** 735–747. [MR2137480](#)
- [38] MÜLLER, H.-G. (2016). Peter Hall, functional data analysis and random objects. *Annals of Statistics* **44** 1867–1887. [MR3546436](#)
- [39] NIETERT, S., GOLDFELD, Z. and KATO, K. (2021). Smooth p-Wasserstein distance: structure, empirical approximation, and statistical applications. In *International Conference on Machine Learning* 8172–8183. PMLR.
- [40] PATRANGENARU, V. and ELLINGSON, L. (2015). *Nonparametric Statistics On Manifolds And Their Applications To Object Data Analysis*. CRC Press. [MR3444169](#)
- [41] PENNEC, X. (2018). Barycentric subspace analysis on manifolds. *Annals of Statistics* **46** 2711–2746. [MR3851753](#)
- [42] PENNEC, X., FILLARD, P. and AYACHE, N. (2006). A Riemannian framework for tensor computing. *International Journal of Computer Vision* **66** 41–66.
- [43] PETERSEN, A. and MÜLLER, H.-G. (2016). Functional data analysis for density functions by transformation to a Hilbert space. *Annals of Statistics*

- 44 183–218. [MR3449766](#)
- [44] PETERSEN, A. and MÜLLER, H.-G. (2019). Fréchet regression for random objects with Euclidean predictors. *Annals of Statistics* **47** 691–719. [MR3909947](#)
- [45] PIGOLI, D., ASTON, J. A., DRYDEN, I. L. and SECCHI, P. (2014). Distances and inference for covariance operators. *Biometrika* **101** 409–422. [MR3215356](#)
- [46] PIGOLI, D., HADJIPANTELOS, P. Z., COLEMAN, J. S. and ASTON, J. A. (2018). The statistical analysis of acoustic phonetic data: exploring differences between spoken Romance languages. *Journal of the Royal Statistical Society: Series C (Applied Statistics)* **67** 1103–1145. [MR3873703](#)
- [47] RAMSAY, J. O. and SILVERMAN, B. W. (2005). *Functional Data Analysis*, 2nd ed. *Springer Series in Statistics*. Springer. [MR2168993](#)
- [48] RAMSAY, J. O. and SILVERMAN, B. W. (2007). *Applied Functional Data Analysis: Methods and Case Studies*. Springer. [MR2168993](#)
- [49] SCARAPICCHIA, V., MAZEROLLE, E. L., FISK, J. D., RITCHIE, L. J. and GAWRYLUK, J. R. (2018). Resting state BOLD variability in Alzheimer’s disease: a marker of cognitive decline or cerebrovascular status? *Frontiers in Aging Neuroscience* **10** 39.
- [50] SCHÖTZ, C. (2020). Strong laws of large numbers for generalizations of Fréchet mean sets. *arXiv preprint arXiv:2012.12762*.
- [51] SENTÜRK, D. and MÜLLER, H.-G. (2010). Functional varying coefficient models for longitudinal data. *Journal of the American Statistical Association* **105** 1256–1264. [MR2752619](#)
- [52] SENTÜRK, D. and NGUYEN, D. V. (2011). Varying coefficient models for sparse noise-contaminated longitudinal data. *Statistica Sinica* **21** 1831–1856. [MR2896001](#)
- [53] SEVERN, K. E., DRYDEN, I. L. and PRESTON, S. P. (2021). Non-parametric regression for networks. *Stat* **10** e373. [MR4276033](#)
- [54] SHI, J. Q., WANG, B., MURRAY-SMITH, R. and TITTERINGTON, D. M. (2007). Gaussian process functional regression modeling for batch data. *Biometrics* **63** 714–723. [MR2395708](#)
- [55] STURM, K.-T. (2003). Probability measures on metric spaces of nonpositive. *Heat Kernels and Analysis on Manifolds, Graphs, and Metric Spaces: Lecture Notes from a Quarter Program on Heat Kernels, Random Walks, and Analysis on Manifolds and Graphs: April 16–July 13, 2002, Emile Borel Centre of the Henri Poincaré Institute, Paris, France* **338** 357. [MR2039961](#)
- [56] TAVAKOLI, S., PIGOLI, D., ASTON, J. A. and COLEMAN, J. S. (2019). A spatial modeling approach for linguistic object data: Analyzing dialect sound variations across Great Britain. *Journal of the American Statistical Association* **114** 1081–1096. [MR4011760](#)
- [57] TURNER, K., MILEYKO, Y., MUKHERJEE, S. and HARER, J. (2014). Fréchet means for distributions of persistence diagrams. *Discrete & Computational Geometry* **52** 44–70. [MR3231030](#)
- [58] VAN DER VAART, A. and WELLNER, J. (2000). *Weak Convergence And Empirical Processes: With Applications To Statistics (Springer Series in*

- Statistics*), Corrected ed. Springer. [MR1385671](#)
- [59] VERZELEN, N., TAO, W. and MÜLLER, H.-G. (2012). Inferring stochastic dynamics from functional data. *Biometrika* **99** 533–550. [MR2966768](#)
- [60] WANG, J.-L., CHIOU, J.-M. and MÜLLER, H.-G. (2016). Functional Data Analysis. *Annual Review of Statistics and its Application* **3** 257–295.
- [61] WANG, L., LI, H. and HUANG, J. Z. (2008). Variable selection in non-parametric varying-coefficient models for analysis of repeated measurements. *Journal of the American Statistical Association* **103** 1556–1569. [MR2504204](#)
- [62] WANG, B. and SHI, J. Q. (2014). Generalized Gaussian process regression model for non-Gaussian functional data. *Journal of the American Statistical Association* **109** 1123–1133. [MR3265685](#)
- [63] WANG, K., LIANG, M., WANG, L., TIAN, L., ZHANG, X., LI, K. and JIANG, T. (2007). Altered functional connectivity in early Alzheimer’s disease: A resting-state fMRI study. *Human Brain Mapping* **28** 967–978.
- [64] WU, C. O. and CHIANG, C.-T. (2000). Kernel smoothing on varying coefficient models with longitudinal dependent variable. *Statistica Sinica* 433–456. [MR1769751](#)
- [65] YANG, C.-H. and VEMURI, B. C. (2020). Shrinkage estimation of the Fréchet mean in Lie groups. *arXiv preprint arXiv:2009.13020*.
- [66] YAO, F., MÜLLER, H.-G. and WANG, J.-L. (2005). Functional data analysis for sparse longitudinal data. *Journal of the American Statistical Association* **100** 577–590. [MR2160561](#)
- [67] YUAN, Y., ZHU, H., STYNER, M., GILMORE, J. H. and MARRON, J. S. (2013). Varying coefficient model for modeling diffusion tensors along white matter tracts. *Annals of Applied Statistics* **7** 102–125. [MR3086412](#)
- [68] ZHANG, J., CLAYTON, M. K. and TOWNSEND, P. A. (2011). Functional concurrent linear regression model for spatial images. *Journal of Agricultural, Biological, and Environmental Statistics* **16** 105–130. [MR2767762](#)
- [69] ZHANG, Q., XUE, L. and LI, B. (2021). Dimension reduction and data visualization for Fréchet regression. *arXiv preprint arXiv:2110.00467*.
- [70] ZHANG, H.-Y., WANG, S.-J., LIU, B., MA, Z.-L., YANG, M., ZHANG, Z.-J. and TENG, G.-J. (2010). Resting brain connectivity: changes during the progress of Alzheimer disease. *Radiology* **256** 598–606.
- [71] ZHOU, J., GREICIUS, M. D., GENNATAS, E. D., GROWDON, M. E., JANG, J. Y., RABINOVICI, G. D., KRAMER, J. H., WEINER, M., MILLER, B. L. and SEELEY, W. W. (2010). Divergent network connectivity changes in behavioural variant frontotemporal dementia and Alzheimer’s disease. *Brain* **133** 1352–1367.
- [72] ZHOU, D., DRYDEN, I. L., KOLOYDENKO, A. A., AUDENAERT, K. M. and BAI, L. (2016). Regularisation, interpolation and visualisation of diffusion tensor images using non-Euclidean statistics. *Journal of Applied Statistics* **43** 943–978. [MR3457097](#)
- [73] ZHU, H., CHEN, Y., IBRAHIM, J. G., LI, Y., HALL, C. and LIN, W. (2009). Intrinsic regression models for positive-definite matrices with applications to diffusion tensor imaging. *Journal of the American Statistical Association*

- 104** 1203-1212. [MR2750245](#)
- [74] ZHU, H., STYNER, M., LI, Y., KONG, L., SHI, Y., LIN, W., COE, C. and GILMORE, J. H. (2010). Multivariate varying coefficient models for DTI tract statistics. In *International Conference on Medical Image Computing and Computer-Assisted Intervention* 690–697. Springer.